AD-A173 141 BIPERIODICITY IN COUPLED-CAVITY TRAVELING-WAVE TUBES (U) UTAH UNIV SALT LAKE CITY DEPT OF ELECTRICAL ENGINEERING S C REICHARD SEP 86 RADC-TR-86-124 1/1

UNCLASSIFIED F/G 9/1 NL

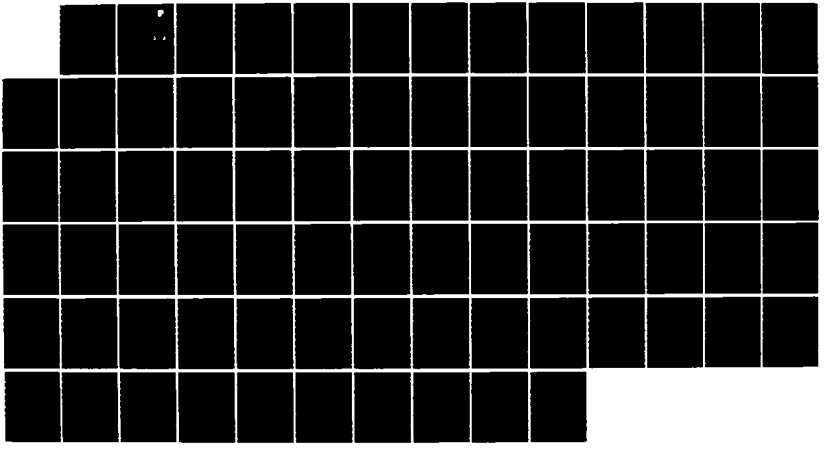

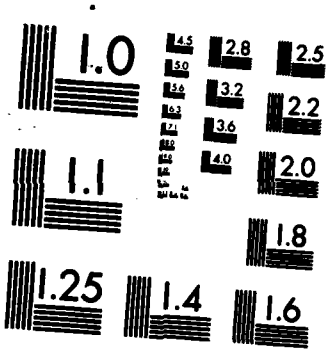

RADC-TR-86-124
Final Technical Report
September 1986

BIPERIODICITY IN COUPLED-CAVITY TRAVELING-WAVE TUBES

University of Utah

Scott C. Reichard

APPROVED FOR PUBLIC RELEASE; DISTRIBUTION UNLIMITED

ROME AIR DEVELOPMENT CENTER
Air Force Systems Command
Griffiss Air Force Base, NY 13441-5700

This report has been reviewed by the RADC Public Affairs Office (PA) and is releasable to the National Technical Information Service (NTIS). At NTIS it will be releasable to the general public, including foreign nations.

RADC-TR-86-124 has been reviewed and is approved for publication.

APPROVED: 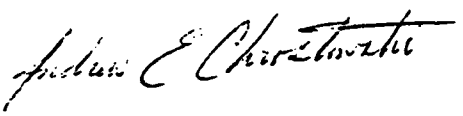

ANDREW E. CHROSTOWSKI, 1Lt, USAF
Project Engineer

APPROVED: 

FRANK J. REHM
Technical Director
Surveillance Division

FOR THE COMMANDER: 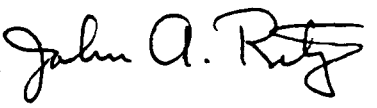

JOHN A. RITZ
Plans and Programs Division

If your address has changed or if you wish to be removed from the RADC mailing list, or if the addressee is no longer employed by your organization, please notify RADC (OCTP) Griffiss AFB NY 13441-5700. This will assist us in maintaining a current mailing list.

Do not return copies of this report unless contractual obligations or notices on a specific document requires that it be returned.

UNCLASSIFIED

SECURITY CLASSIFICATION OF THIS PAGE

REPORT DOCUMENTATION PAGE

1a. REPORT SECURITY CLASSIFICATION UNCLASSIFIED	1b. RESTRICTIVE MARKINGS N/A
2a. SECURITY CLASSIFICATION AUTHORITY N/A	3. DISTRIBUTION/AVAILABILITY OF REPORT Approved for public release; distribution unlimited
2b. DECLASSIFICATION/DOWNGRADING SCHEDULE N/A	
4. PERFORMING ORGANIZATION REPORT NUMBER(S) N/A	5. MONITORING ORGANIZATION REPORT NUMBER(S) RADC-TR-86-124
6a. NAME OF PERFORMING ORGANIZATION University of Utah 6b. OFFICE SYMBOL (If applicable)	7a. NAME OF MONITORING ORGANIZATION Rome Air Development Center (OCTP)
6c. ADDRESS (City, State, and ZIP Code) Department of Electrical Engineering Salt Lake City UT 84112	7b. ADDRESS (City, State, and ZIP Code) Griffiss AFB NY 13441-5700
8a. NAME OF FUNDING/SPONSORING ORGANIZATION AFOSR 8b. OFFICE SYMBOL (If applicable) NE	9. PROCUREMENT INSTRUMENT IDENTIFICATION NUMBER F30602-82-C-0161
8c. ADDRESS (City, State, and ZIP Code) Bolling AFB Wash DC 20332	10. SOURCE OF FUNDING NUMBERS PROGRAM ELEMENT NO. 61102F; PROJECT NO. 2305; TASK NO. J9; WORK UNIT ACCESSION NO. 16
11. TITLE (Include Security Classification) BIPERIODICITY IN COUPLED-CAVITY TRAVELING-WAVE TUBES	
12. PERSONAL AUTHOR(S) Scott C. Reichard	
13a. TYPE OF REPORT Final 13b. TIME COVERED FROM Sep 82 TO Sep 85	14. DATE OF REPORT (Year, Month, Day) September 1986 15 PAGE COUNT 84
16. SUPPLEMENTARY NOTATION N/A	

17. COSATI CODES			18. SUBJECT TERMS (Continue on reverse if necessary and identify by block number)
FIELD	GROUP	SUB-GROUP	
09	03		Biperiodicity; Brillouin Diagrams; Coupled-Cavity; Curnow Equivalent-Circuit Cells; TWT
10	02		

19. ABSTRACT (Continue on reverse if necessary and identify by block number)

This study concerns analysis of wave propagation in coupled-cavity traveling-wave tube (CCTWT) interaction structures having the feature of biperiodicity: The alternating between two different geometries of consecutive resonators or coupling interfaces or both. Brillouin diagrams are computed and discussed for a number of existing and proposed biperiodic circuit structures. A better understanding of propagation in biperiodic structures is valuable because:

1. A biperiodic structure can provide a unique w-B curve with features benefiting "hot" bandwidth and stability.

2. A nonbioperiodic structure can become biperiodic through fabrication deficiencies with consequences determintal to tube performance.

3. Some nonbioperiodic CCTWT structures are biperiodic with respect to spurious higher-order modes resulting in interference detrimental to tube operation. (over)

20. DISTRIBUTION/AVAILABILITY OF ABSTRACT ☒ UNCLASSIFIED/UNLIMITED ☐ SAME AS RPT ☐ DTIC USERS	21. ABSTRACT SECURITY CLASSIFICATION UNCLASSIFIED
22a. NAME OF RESPONSIBLE INDIVIDUAL Andrew E. Chrostowski, 1Lt, USAF	22b. TELEPHONE (Include Area Code) (315) 330-4381 22c. OFFICE SYMBOL RADC (OCTP)

DD FORM 1473, 84 MAR 83 APR edition may be used until exhausted. All other editions are obsolete.

SECURITY CLASSIFICATION OF THIS PAGE

UNCLASSIFIED

Block 19. Abstract (Cont'd)

The computer-assisted analysis is based on Curnow equivalent-circuit cells resulting in the ability to model existing biperiodic structures, to design new structures utilizing the benefits of biperiodicity and to better understand biperiodicity resulting from mechanical defects or relevant to spurious higher-order modes when present in a conventional periodic structure.

ACKNOWLEDGEMENTS

I would like to especially express my gratitude to Dr. Arthur Karp for his supervision of this project and for his many suggestions and insights. I would like additionally to thank Mr. Dave Aster for his valuable contribution of computer programs and patient explanations. This study would not have been possible without the support of the Air Force Thermionic Research program and Varian Associates.

TABLE OF CONTENTS

LIST OF ILLUSTRATIONS AND TABLES

I. INTRODUCTION

This study pertains to slow-wave interaction structures of traveling-wave tubes other than those based on helices. These periodic structures are viewed as consisting of alternating interfaces and resonators with a combination of an interface and adjacent resonator defined as one cell. Each cell in a standard periodic structure is identical to all others (Fig. 1a). In a biperiodic structure the cells alternate between two different cell types, A and B (Fig. 1b), with the differences between A and B being either large or small. Staggering coupling slots from one interface to another does not constitute biperiodicity as considered in this study. The electron beam of the TWT is always assumed to traverse all cells.

An understanding of the electromagnetic properties of biperiodic TWT interaction structures and the ability to model them analytically is important for several reasons. Accidental biperiodicity may occur in a standard periodic TWT as a result of certain fabrication deficiencies, particularly when the wavelength and physical dimensions are very small. Since the Brillouin diagram of a biperiodic TWT has stopbands in addition to those of a standard TWT, accidental biperiodicity, corresponding to only small differences between adjacent cells, adds narrow stopbands centered at frequencies for which $\beta L = n\pi/2$ (n is odd) [1,2]. Because these narrow stopbands can be detrimental to tube performance, understanding the phenomenon facilitates alleviating the problems.

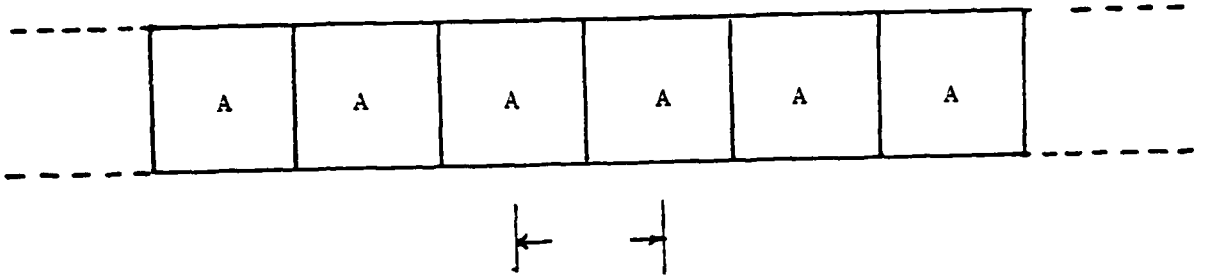

(a)

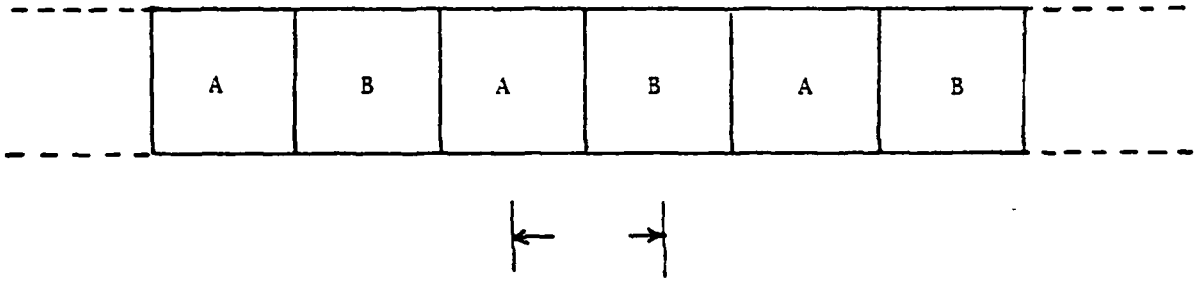

(b)

Fig. 1. Periodic structures (schematic).
a. Standard
b. Biperiodic

A second reason is the useful dispersion characteristics of the Brillouin diagrams of some intentionally biperiodic interaction structures. Figure 2 shows partial Brillouin diagrams in three categories based on actual tube structures. The ω-β curves of Fig. 2a and 2b show, respectively, high and moderate dispersion and low and moderate potential "hot" (instantaneous) bandwidths. In Fig. 2c, showing a portion of the Brillouin diagram that some biperiodic structures can provide, the "cold" bandwidth can be narrower than in Fig. 2a, but the dispersion characteristics can promote a wider "hot" bandwidth. Additionally the flatness of the upper portion of the curve promotes tube stability through decreased band-edge oscillation tendencies. Two intentionally biperiodic TWTs have been successfully operated: a 29 GHz TWT recently developed by Varian Canada, Inc. [3] (see also Fig. 3) uses differences between the resonators of cells A and B; an X-band TWT developed some time ago at Stanford University [4] (see also Fig. 4) relies on differences between successive interfaces.

A third way that research on biperiodic circuit structures can be of benefit involves spurious higher-order modes in a standard periodic structure such as the one shown in Fig. 5a [5]. While the structure is not biperiodic for the useful mode of propagation, from time to time production CCTWTs of this and other types have been observed to suffer from interference from a higher-order mode of propagation. It can be shown that this particular mode propagates as if there were a conducting septum running through the tube as shown in Fig. 5b. Looking on either side of the septum, it is seen that the coupling interfaces are both staggered and biperiodic.

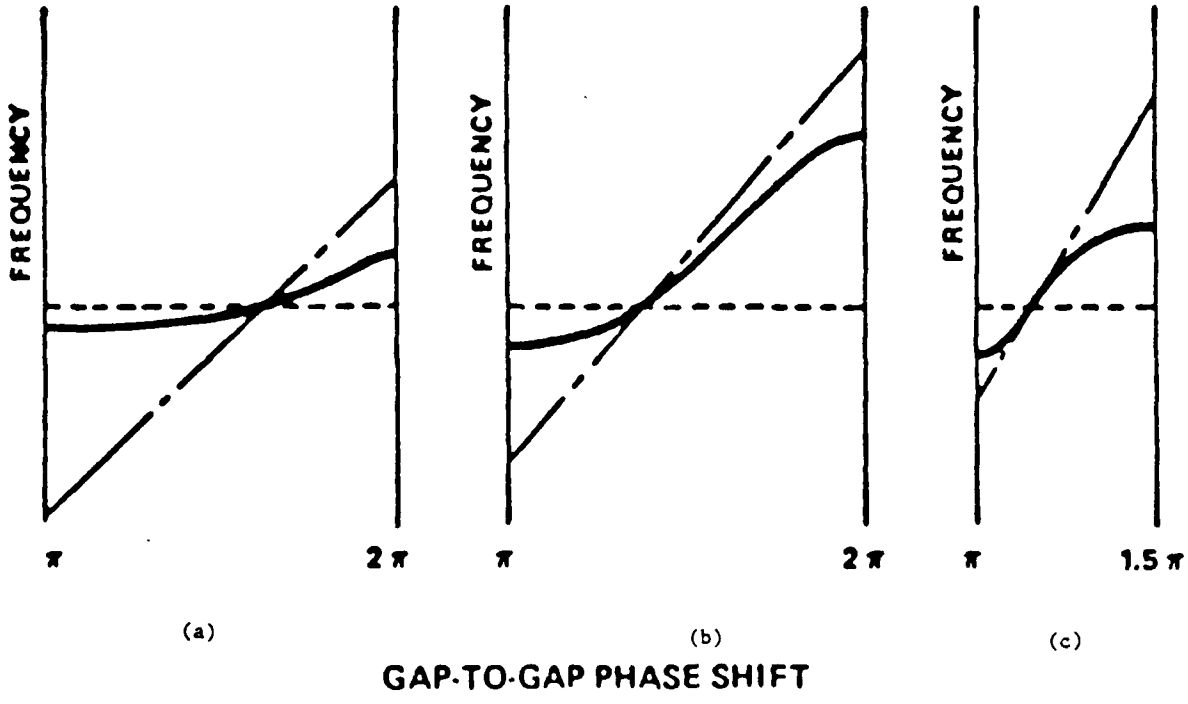

Fig. 2. Dispersion curves of different periodic interaction structures.
a. Conventional in-line coupled-cavity chain.
b. Conventional staggered coupled-cavity chain.
c. Biperiodic in-line structure.

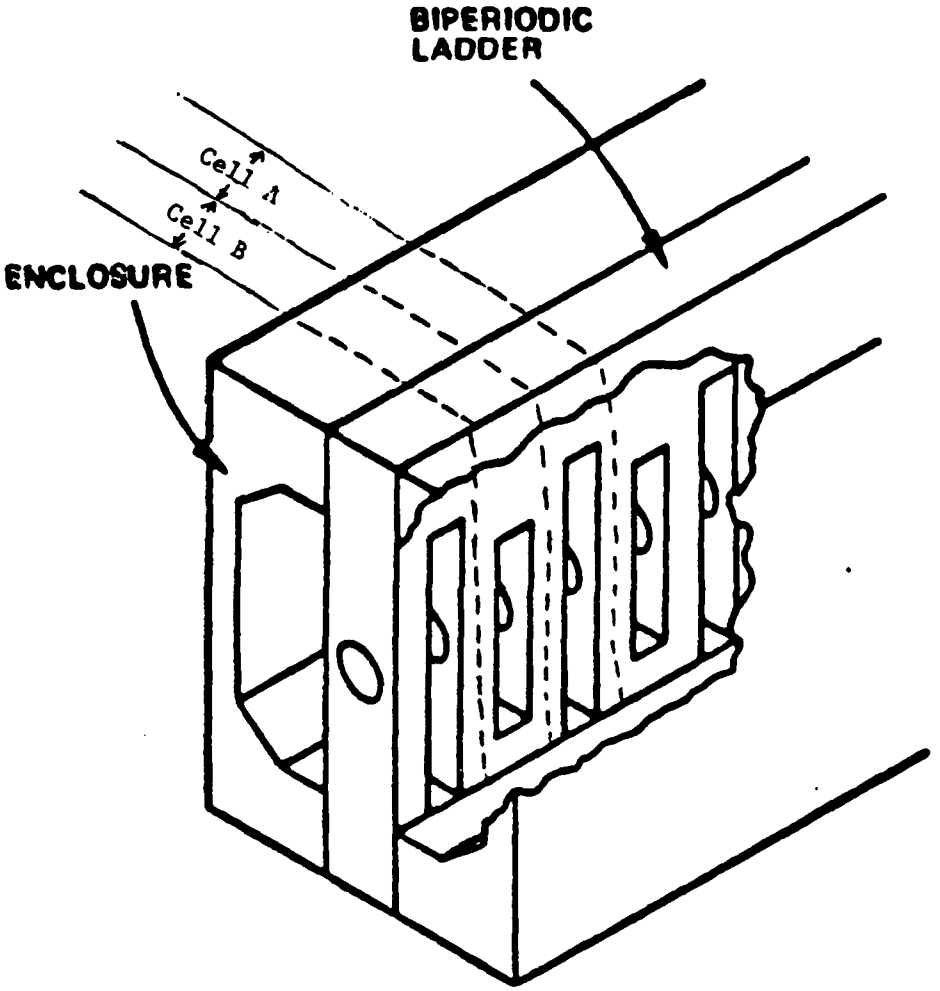

Fig. 3. Biperiodic free-ladder interaction structure.

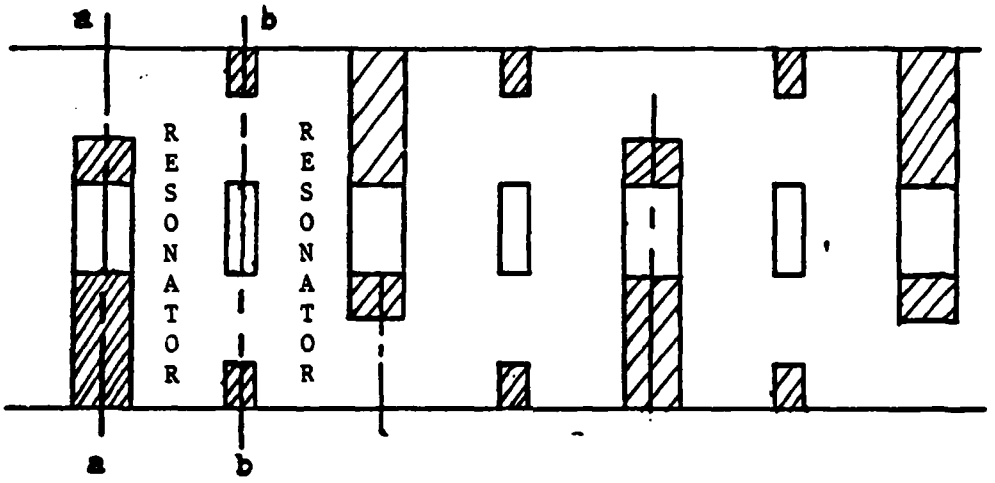

Longitudinal section of structure

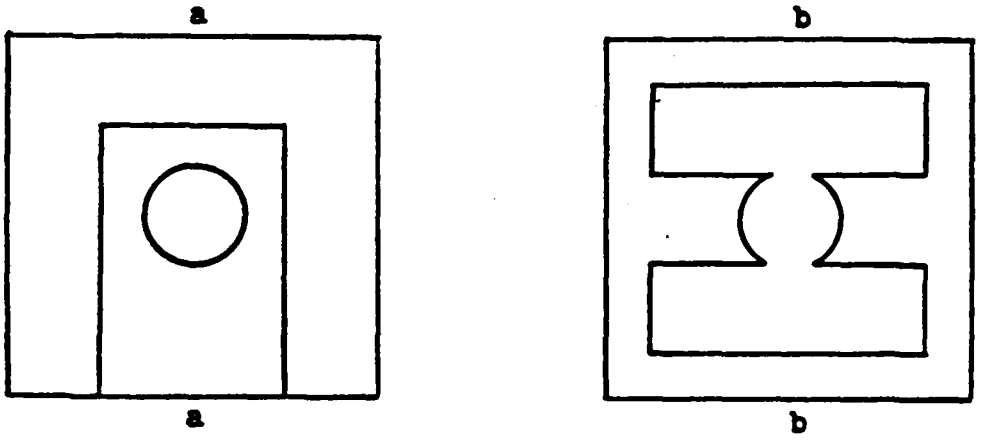

INTERFACE A

INTERFACE B

Fig. 4. TWT structure used by B. Arfin [4] viewed as a chain of equal resonators with two alternating types of interfaces.

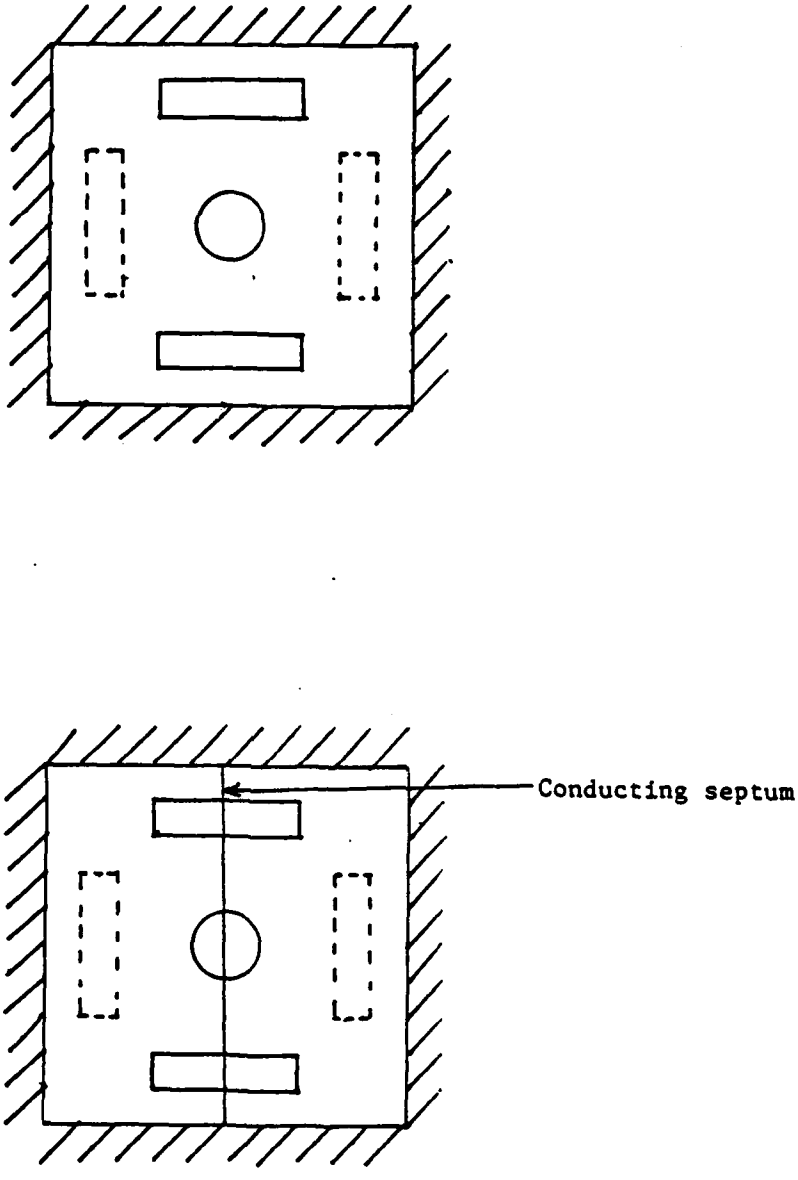

Fig. 5. Simplified end view of a familiar coupled-cavity interaction structure.
a. Actual structure
b. Effective structure for a higher-order mode

II. PERIODIC STRUCTURES

A periodic transmission system is a filter structure with alternating bands of frequencies of high attenuation (stopbands) and of little or no attenuation (passbands). A plot (Brillouin diagram) of angular frequency (ω) versus the phase change per unit of length (β) clearly depicts both of these types of bands (Fig. 6). With CCTWT amplifiers the emphasis is on the lowest passband because these tubes cannot easily make use of higher passbands. Consequently, the Brillouin diagrams in this report will often show only the lowest passband even though others exist. Whether a structure can lead to a narrow- or wide-band tube is implied in these diagrams. The "cold" bandwidth, in percent, of a passband with a high-frequency edge F_2 and a low-frequency edge F_1 is

$$BW_c = [2(F_2 - F_1)/(F_2 + F_1)] \ (100).$$

The "hot" bandwidth is the instantaneous tube operating bandwidth within a useful passband. The endpoints of the "hot" bandwidth are the frequencies (F_4 and F_3; $F_4 < F_2$ and $F_3 > F_1$) where the tube gain is 3 dB down (usually) from the maximum gain. The "hot" bandwidth is

$$BW_H = [2(F_4 - F_3)/(F_4 + F_3)] \ (100).$$

Conventional CCTWTs tend to use the $1 < \beta L/\pi < 2$ interval because it is a good compromise between the high voltage and narrow "hot" bandwidth

associated with a lower range ($0 < \beta L/\pi < 1$) and the low effective interaction impedance associated with a higher range ($\beta L/\pi > 2$). The interval between $0 < \beta L/\pi < 1$ indicates fundamental or non-space-harmonic operation while $\beta L/\pi > 1$ indicates space-harmonic operation.

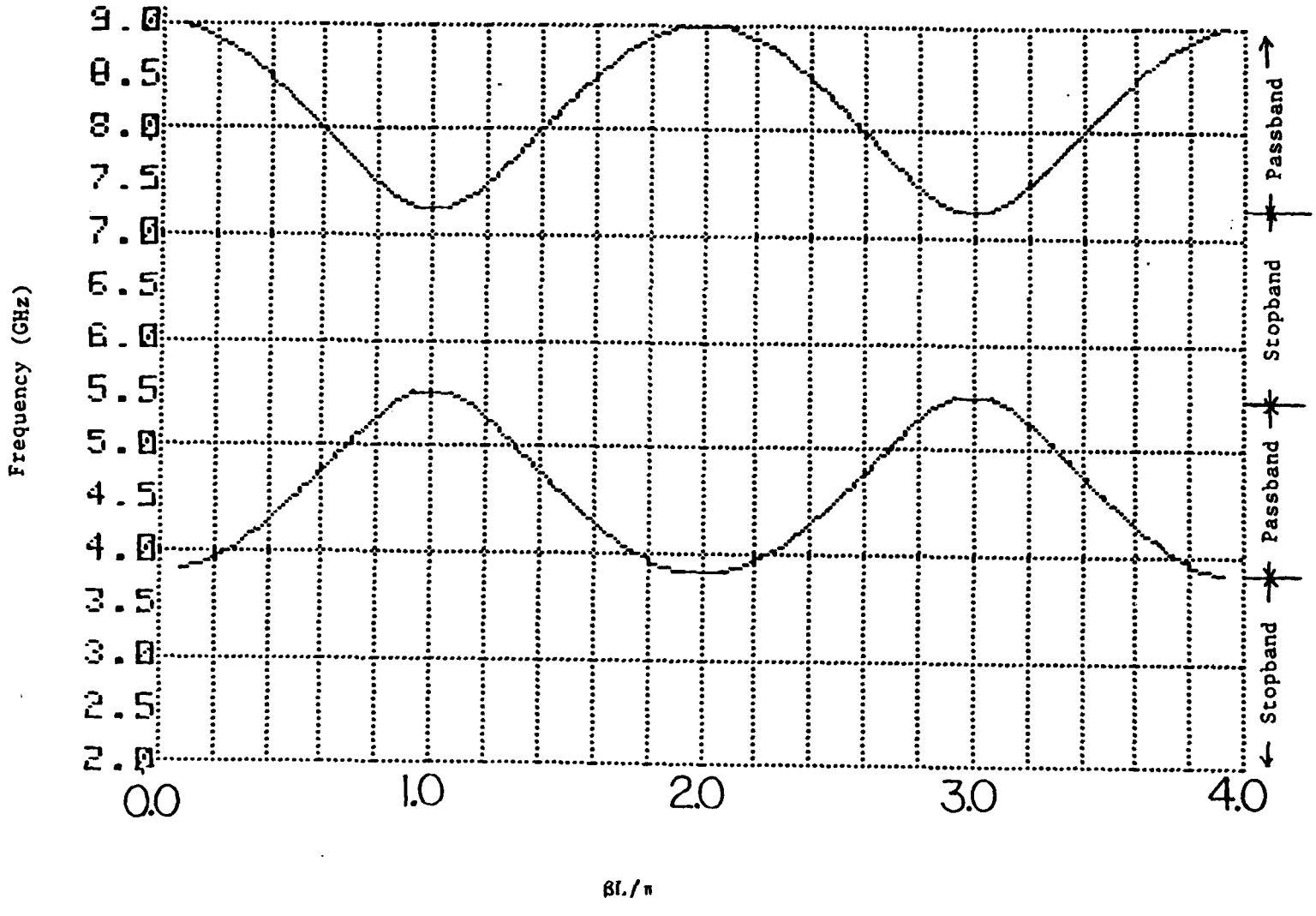

Fig. 6. Sample Brillouin diagram showing stopbands and passbands.

III. CURNOW CELLS

One method of modeling a periodic coupled-cavity TWT structure is the concentration of lumped-element cells each referred to as a Curnow cell [6]. In this approach, the central resonator and the interface are each modeled as a parallel capacitor-inductor combination (Fig. 7). For illustration purposes a structure is used having a chain of simple klystron type cavities with identical coupling slots in between. Figure 8 shows the complete Curnow equivalent circuit. Since each coupling-slot resonator is shared by two cavities, L_3 and C_3 are split into their parallel components $C_3/2$ and $2L_3$. C_1 is the capacitance related to the interaction gap and L_C is associated with the currents in the cavity walls such that it resonates with C_1 at the cavity resonance frequency. In Fig. 9 the RF current *flow* external to C_1 and completing the loop from one side of C_1 to the other is divided into four parts. The fraction of this flow not intercepting any coupling slots and not involved in coupling to other cavities is p. The fraction intercepting one slot only and involved in coupling to one adjacent cavity is designated by m. The fraction intercepting both slots and involved in coupling to both adjacent cavities is n. These four parts correspond to four parallel inductors which form L_C when combined. They are

$$L_1 = L_C/p$$

$$L_{2A} = L_C/m_A$$

$$L_{2B} = L_C/m_B$$

$$L_9 = L_C/n$$

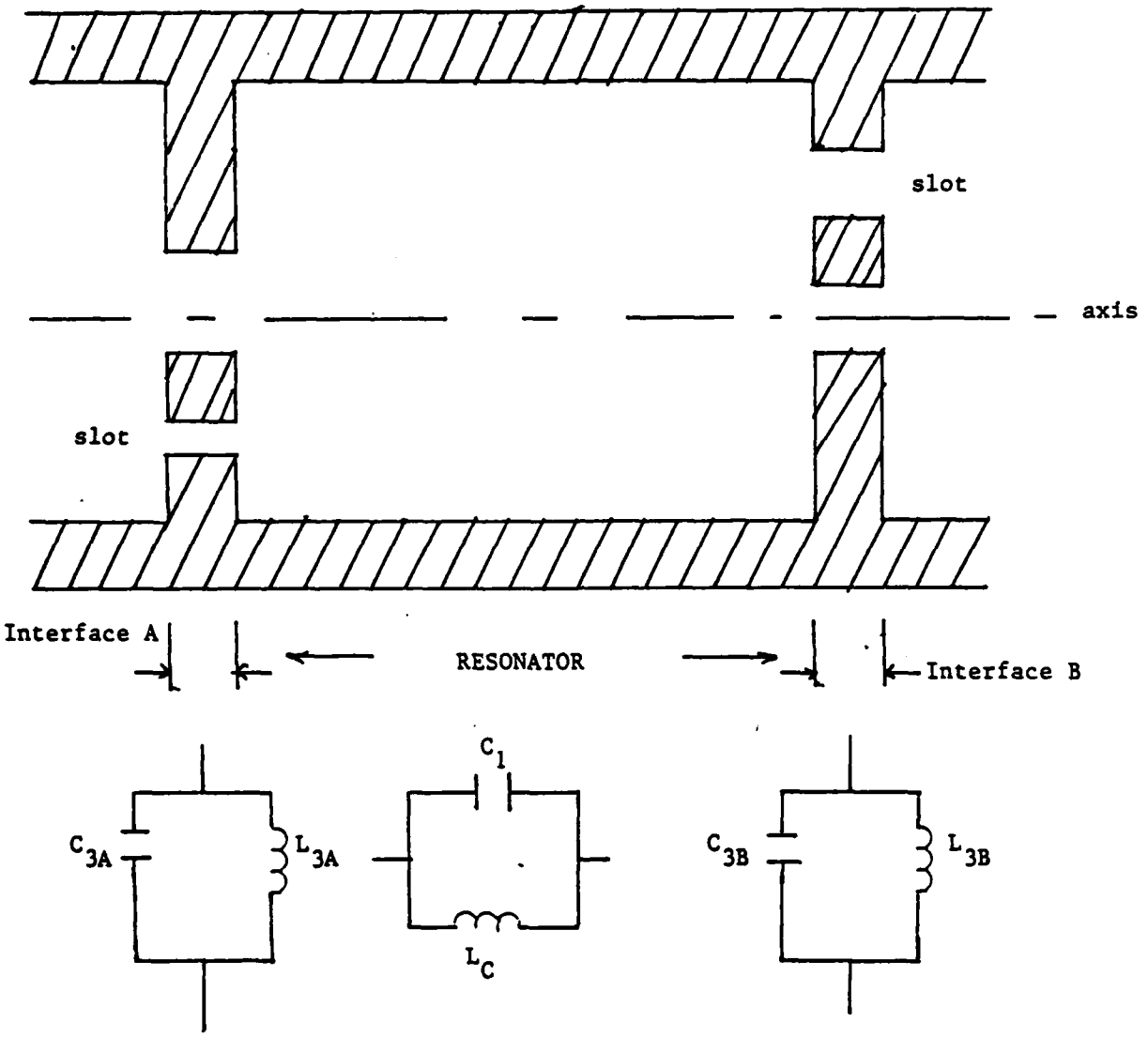

Fig. 7. Resonator and interface equivalent-circuit components.

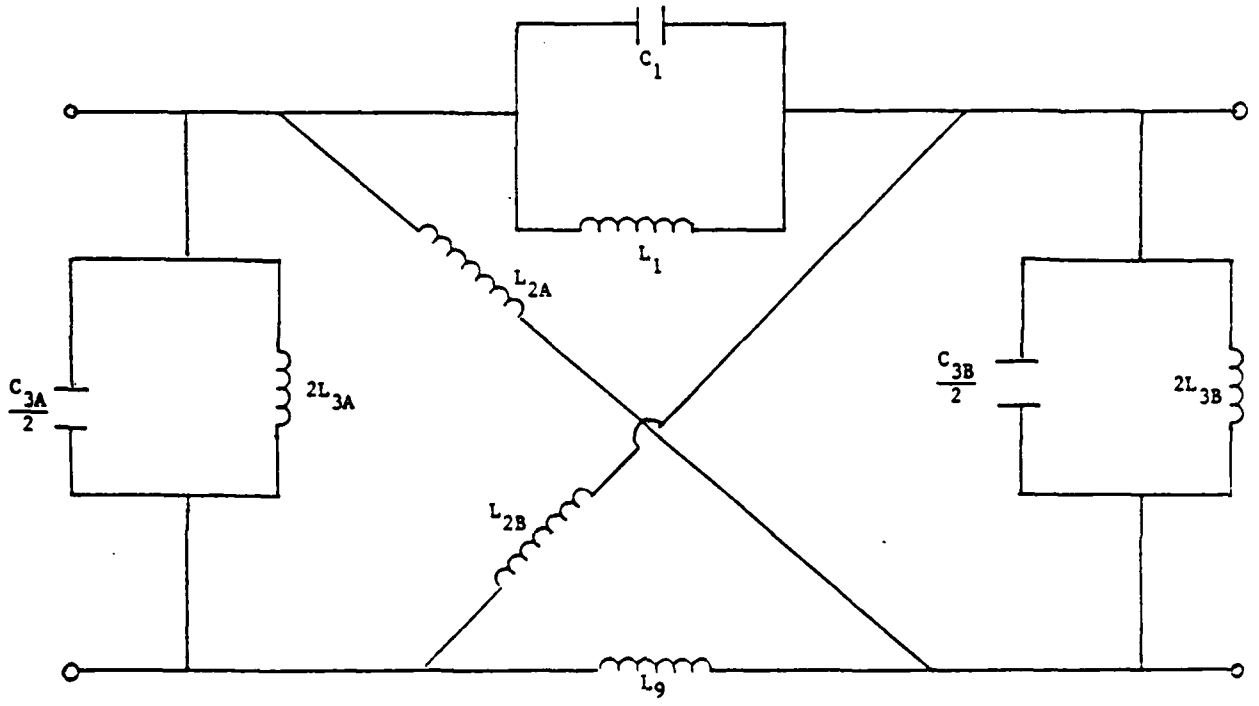

Fig. 8. Individual Curnow cell.

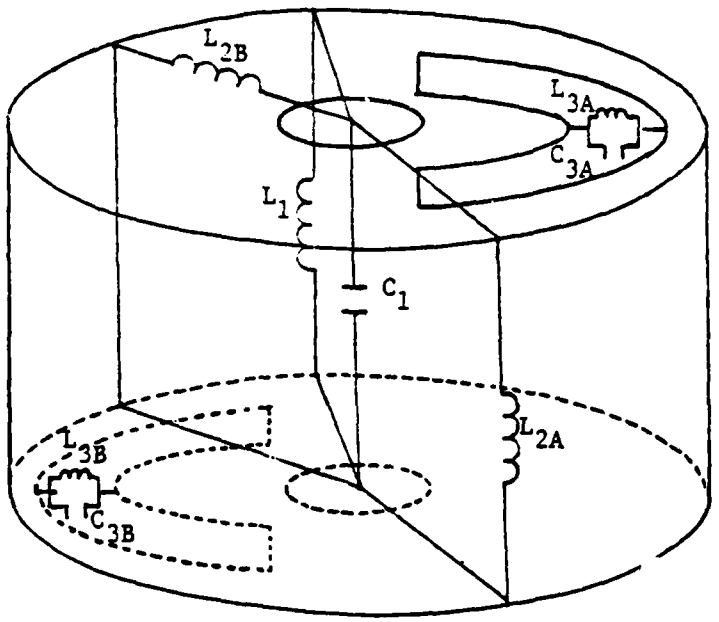

Fig. 9. Division of RF cavity current into portions flowing through L_{2A}, L_{2B}, and L_1. (L_9 and portion of current through it are not significant in this case, though they would be if C_{3A} and L_{3A} were on the same side of the axis as C_{3B} and L_{3B}.)

Putting two cells together, representing two adjacent resonators and interfaces, allows the modeling of all types of biperiodic structures (Fig. 10).

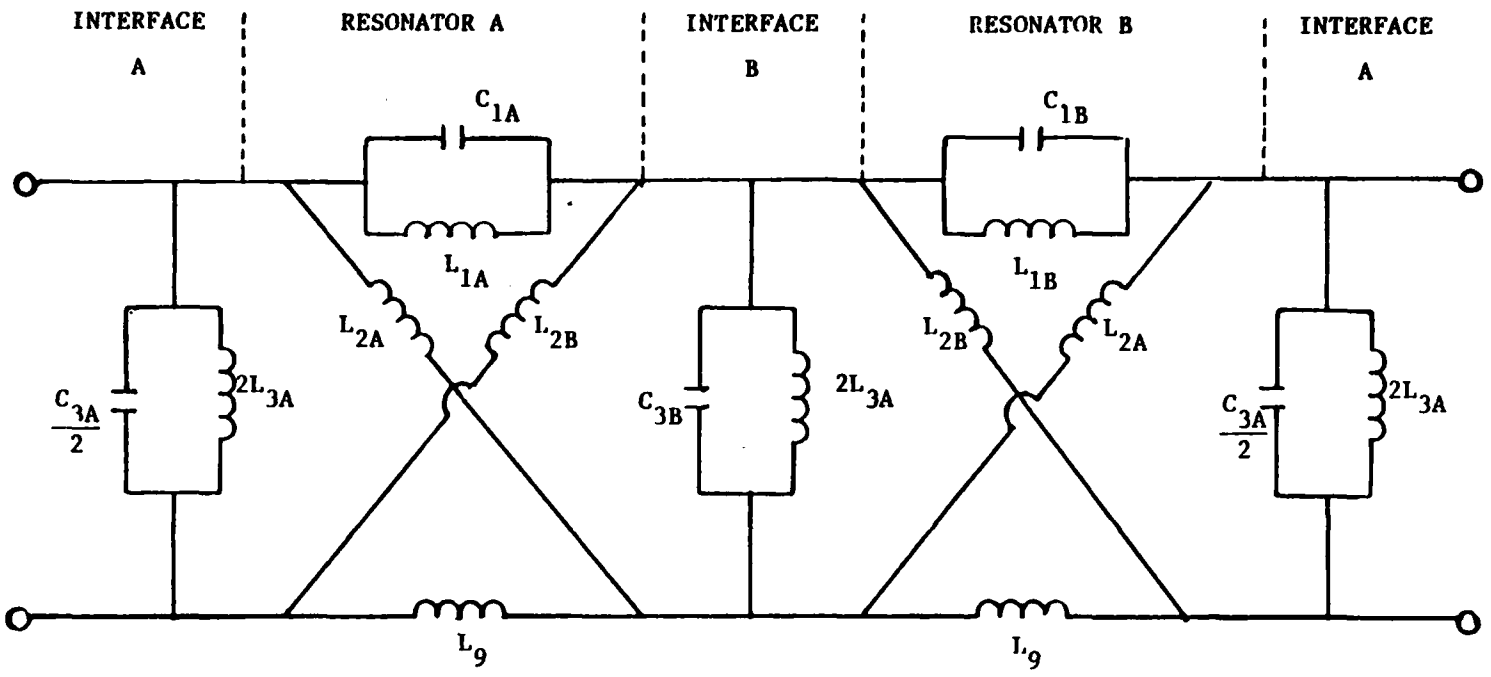

Fig. 10. Two Curnow cells for modeling biperiodic structures.

IV. BIPERIODICITY

If a standard periodic structure is viewed as a sequence of resonators joined by interfaces, then a biperiodic structure is created by alternating consecutive interfaces or resonators or both between two different geometries, a process referred to here as biperiodic "modulation". Resonator modulation produces gap voltages that alternate between two values, but the gap-to-gap phase shift remains constant along the tube. Interface modulation produces constant gap voltages (except for the effects of electronic gain and ohmic loss), but the gap-to-gap phase shift alternates between two values [1].

Both interfaces and resonators can be modulated in frequency or in impedance. The resonance frequency of each resonator of the approximating circuit is given by

$$F_R = (4\pi^2 C_1 L_C)^{-1/2}$$

where L_C is defined as the parallel combination of L_{2A}, L_{2B}, L_9, and L_1. The interaction-gap impedance is given by

$$Z_R = (L_C/C_1)^{1/2}.$$

Each coupling interface has an associated resonance frequency

$$F_I = (4\pi^2 C_3 L_3)^{-1/2}$$

and impedance

$$Z_I = (L_3/C_3)^{1/2}. \qquad [5]$$

Alternating the product C_1L_C between two values modulates the resonator frequency and alternating the ratio L_C/C_1 modulates the resonator impedance. The same holds for modulation of the interface frequency (L_3C_3) and impedance (L_3/C_3). All sixteen possible basic combinations are listed in Table 1. Where two or more parameters are being modulated, one of the modulations may be implemented in the same or opposite sense as the other making a total of 41 possibilities.

Table 1. Options for modulation of cell parameters.

Parameters Modulated

F_I = Interface frequency

Z_I = Interface impedance

F_R = Resonator frequency

Z_R = Resonator impedance

		(C_1L_C) Constant		(C_1L_C) Modulated	
		(C_3L_3) Constant	(C_3L_3) Modulated	(C_3L_3) Constant	(C_3L_3) Modulated
$\frac{L_C}{C_1}$ Constant	$\frac{L_3}{C_3}$ Constant	Standard Periodic Tube	F_I	F_R	F_I, F_R
	$\frac{L_3}{C_3}$ Modulated	Z_I	F_I, Z_I	F_R, Z_I	F_I, F_R, Z_I
$\frac{L_C}{C_1}$ Modulated	$\frac{L_3}{C_3}$ Constant	Z_R	F_I, Z_R	F_R, Z_R	F_I, F_R, Z_R
	$\frac{L_3}{C_3}$ Modulated	Z_R, Z_I	F_I, Z_R, Z_I	F_R, Z_R, Z_I	F_I, F_R, Z_I, Z_R

V. CALCULATING BRILLOUIN DIAGRAMS

The main effort of this project was to develop and use Curnow equivalent circuits to calculate Brillouin diagrams from which much information can be obtained about wave propagation in an interaction structure. For various periodic circuit structures, and for various degrees of modulation in each, this information is obtained and the kinds of tubes that might make use of such structures determined. This work did not include any calculations regarding interaction impedance, electronic gain, or ohmic loss, but the Curnow circuits that were developed can be readily used for these purposes in the future.

Two basic structure cases were examined and Fig. 11 shows their geometries for the unmodulated state. The free-ladder interaction structure (Fig. 11a) has a ladder element with equal rung widths and aperture lengths surrounded by an enclosure. The familiar coupled-cavity circuit of Fig. 11b has staggered coupling slots that all subtend $\psi = 160°$.

The initial unmodulated element values are given in Table 2. The free-ladder Curnow elements were calculated from cold-test scale-model measurements. The method for doing this is reviewed by Darbin [7]. The staggered coupled-cavity Curnow elements were arrived at by visualizing a representative physical cavity (as opposed to cold test measurements). From its resonance frequency and R/Q, the values of C_1 and L_C are calculated. L_{2A}, L_{2B}, L_1, and L_9 are calculated from estimates of the respective fractions of the cavity circulating current. A physical coupling slot is visualized and its frequency and impedance are esti-

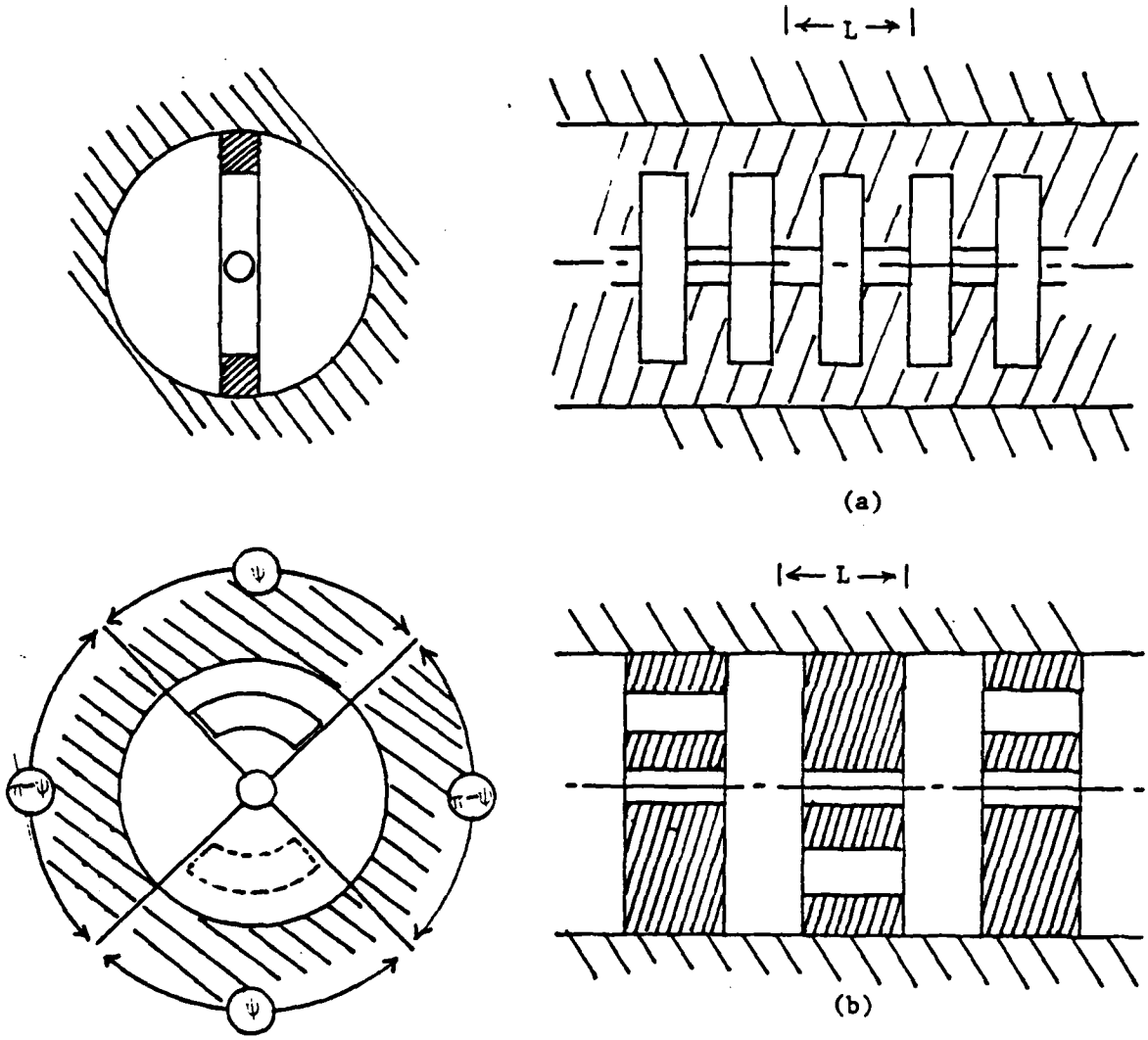

Fig. 11. Basic interaction structures.
a. Free ladder (in enclosure).
b. Coupled cavities with staggered coupling.

Table 2. Curnow circuit elements for unmodulated structures studied.

		Structure of Fig. 11a	Structure of Fig. 11b
L_1	(nH)	3.082	4.7747
C_1	(pF)	1.038	.58946
L_3	(nH)	4.032	3.1831
C_3	(pF)	1.016	.31831
L_9	(nH)	7.54	500.000
$L_{2A} = L_{2B}$	(nH)	109.37	1.1937

mated and from that C_3 and L_3 are derived. The calculations for the Curnow elements for the structure in Fig. 11b are given in Appendix A.

Brillouin diagrams may be obtained by plotting the values of β computed for each frequency. β may be solved from the transmission line of Fig. 10. A matrix of impedances and input and output voltages and currents is established: [8]

$$\begin{bmatrix} V_{OUT} \\ I_{OUT} \end{bmatrix} = \begin{bmatrix} A & B \\ C & D \end{bmatrix} \begin{bmatrix} V_{IN} \\ I_{IN} \end{bmatrix}$$

A, B, C, and D are terms derived from the transmission line sections. Rewriting this system as

$$\lambda \begin{bmatrix} V_{IN} \\ I_{IN} \end{bmatrix} = \begin{bmatrix} A & B \\ C & D \end{bmatrix} \begin{bmatrix} V_{IN} \\ I_{IN} \end{bmatrix}$$

and solving for the eigenvalues (λ) of the system for each frequency enables β, the phase of the eigenvalue (λ), to be calculated. The specifics of these calculations are given in Appendix B. Software developed by D. Aster was used for the actual calculations and to provide the Brillouin diagrams.

VI. RESULTS: BIPERIODIC FREE-LADDER STRUCTURE

A. Original Unmodulated Structure

The first case investigated is the periodic free-ladder interaction structure of Fig. 11a. Physically the resonator is the volume between two transverse planes bisecting adjacent ladder rungs. The dominant element of this resonator is the ladder opening between the rungs. The coupling interface is a plane passing transversely through a rung and containing the two flanking in-line coupling slots. Figure 12 is the Brillouin diagram for the lowest passband of an actual structure without any biperiodic modulation. Higher passbands exist and their curves respond to biperiodic modulation in a similar manner to that of the lowest passband. These higher passbands are omitted for simplicity and clarity. The initial values of the Curnow cell elements are calculated from cold-test scale-model measurements [7]. There is no present interest in basing a practical amplifier on this unmodulated structure, which would have to make use of either the zero-order or the second-order space harmonics ($0 < \beta/\pi < 1$ and $2 < \beta L/\pi < 3$, respectively). In the former interval the beam voltage and dispersion are much too high and in the latter interval the space-harmonic interaction impedance is much too low.

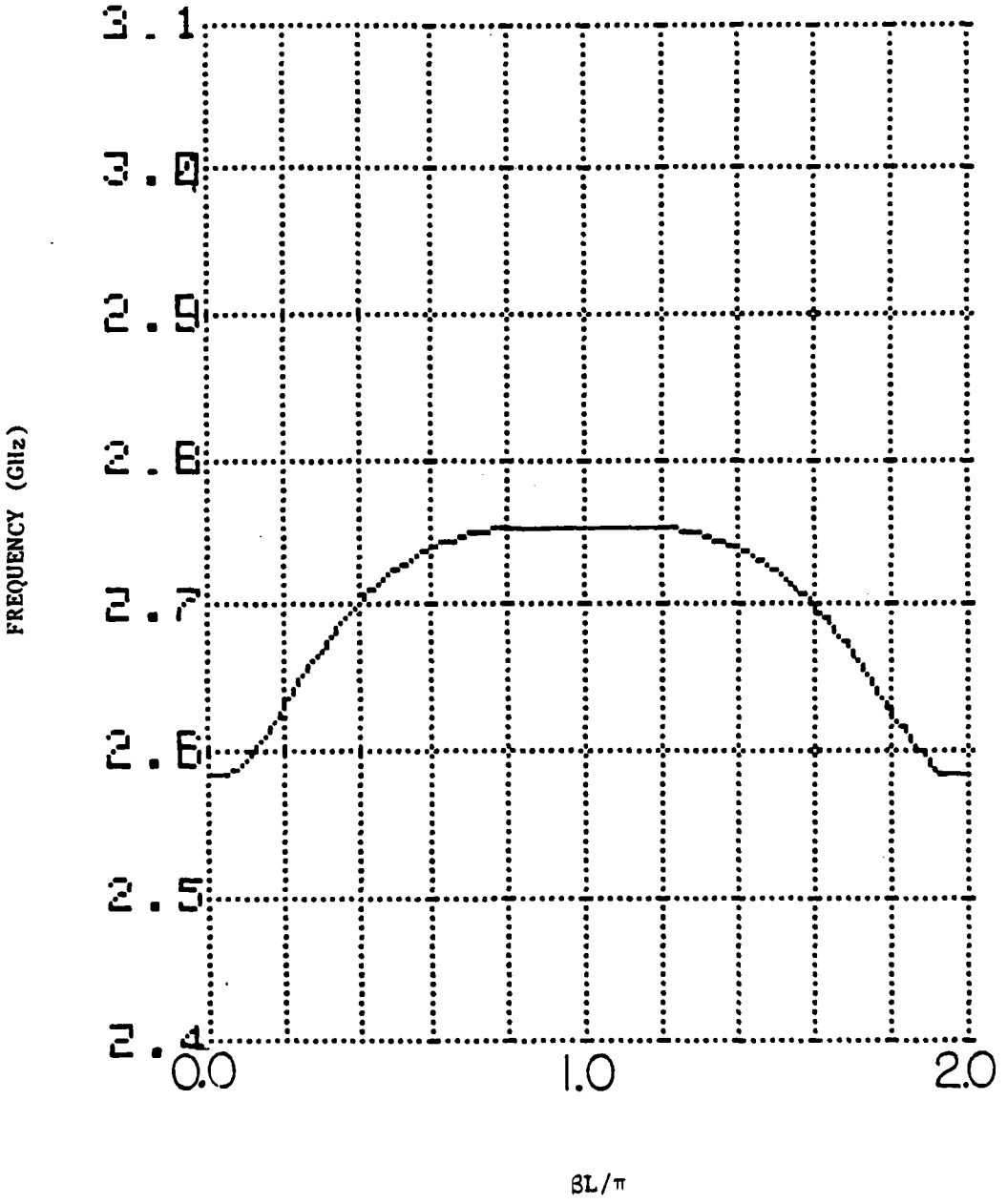

Fig. 12. Brillouin diagram for structure of Fig. 11a. (lowermost passband only)

B. Biperiodic Modulation of Coupling Interface Frequency

The first type of biperiodic modulation to be discussed is that of the interface frequency. In the chain of Curnow cells, this is implemented by multiplying L_{3A} and C_{3A} and dividing L_{3B} and C_{3B} by the same modulation factor, M, of the form $(1 + \delta)$. With δ very small ($\delta = 0.03$ and $M = 1.03$) a small stopband occurs (Fig. 13) between 2.7 GHz and 2.75 GHz centered at 2.72 GHz, the frequency for which $\beta L/\pi = 0.5$ before the introduction of biperiodic modulation. The splitting of one passband to form two passbands in the range of frequencies covered in Fig. 13 is accompanied by a doubling of the number of space harmonics in a given interval of βL [9]. An amplifier based on the lowest branch of the ω-β curve and the $1 < \beta L/\pi < 1.5$ space harmonic could be considered if the dispersion were not so high ("cold" bandwidth is only 4.3 percent). A further increase in M results in an even more dispersive lower passband. (The implementation of this kind of modulation in a physical structure is probably impractical and beyond the scope of this study.)

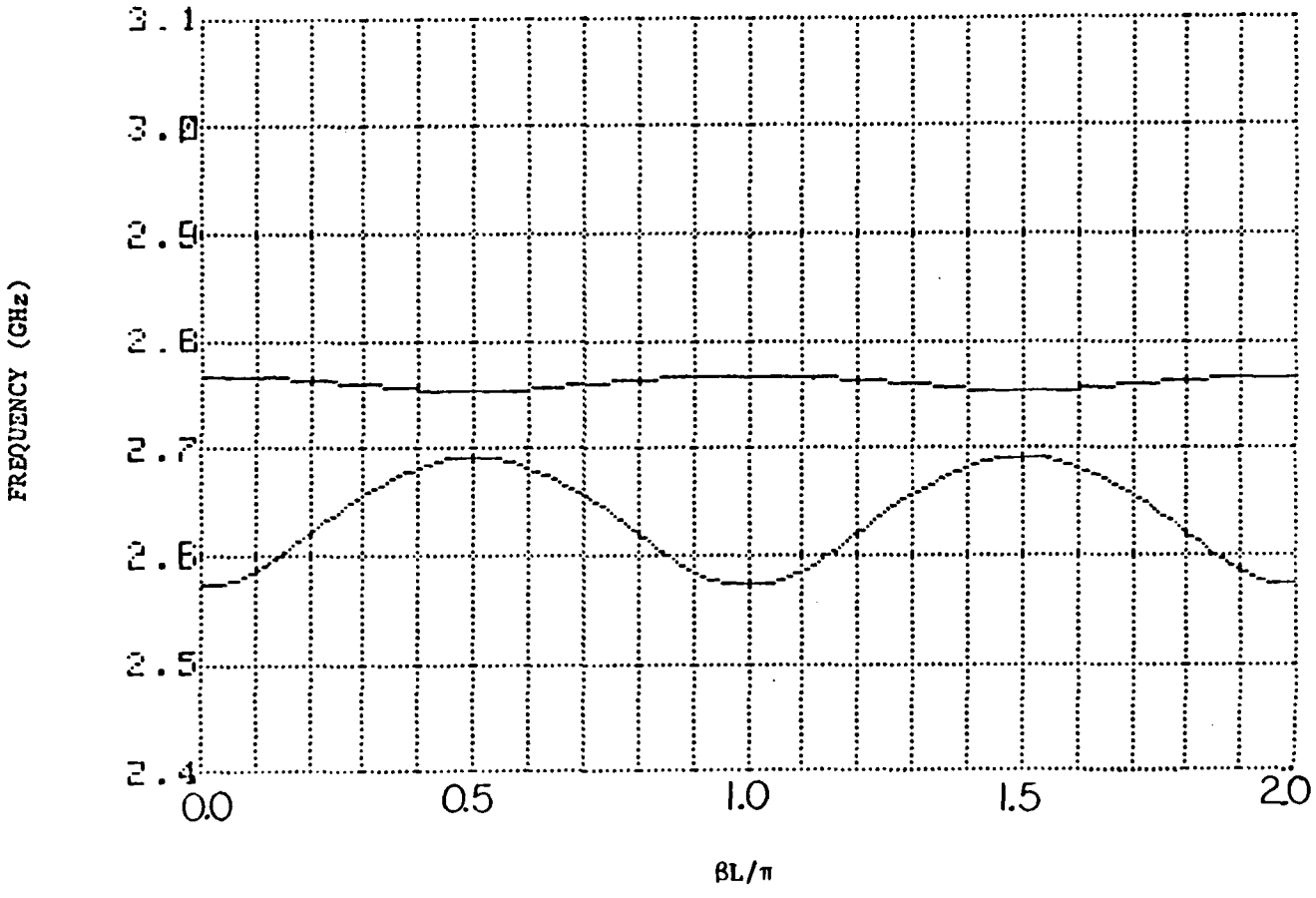

Fig. 13. Brillouin diagram obtained with interface frequency modulation (M = 1.0).

C. Biperiodic Modulation of Coupling Interface Impedance

In the next phase of the study the interface impedance is modulated biperiodically in the Curnow chain by multiplying L_{3B} and C_{3A} and dividing L_{3B} and C_{3A} by M. In the physical structure this kind of modulation might be effectively achieved with alternately thick and thin ladder rungs. With M = 1.03, a narrow stopband centered at 2.72 GHz (Fig. 14) is produced. As seen in Fig. 15, increasing M to 1.10 narrows both passbands slightly.

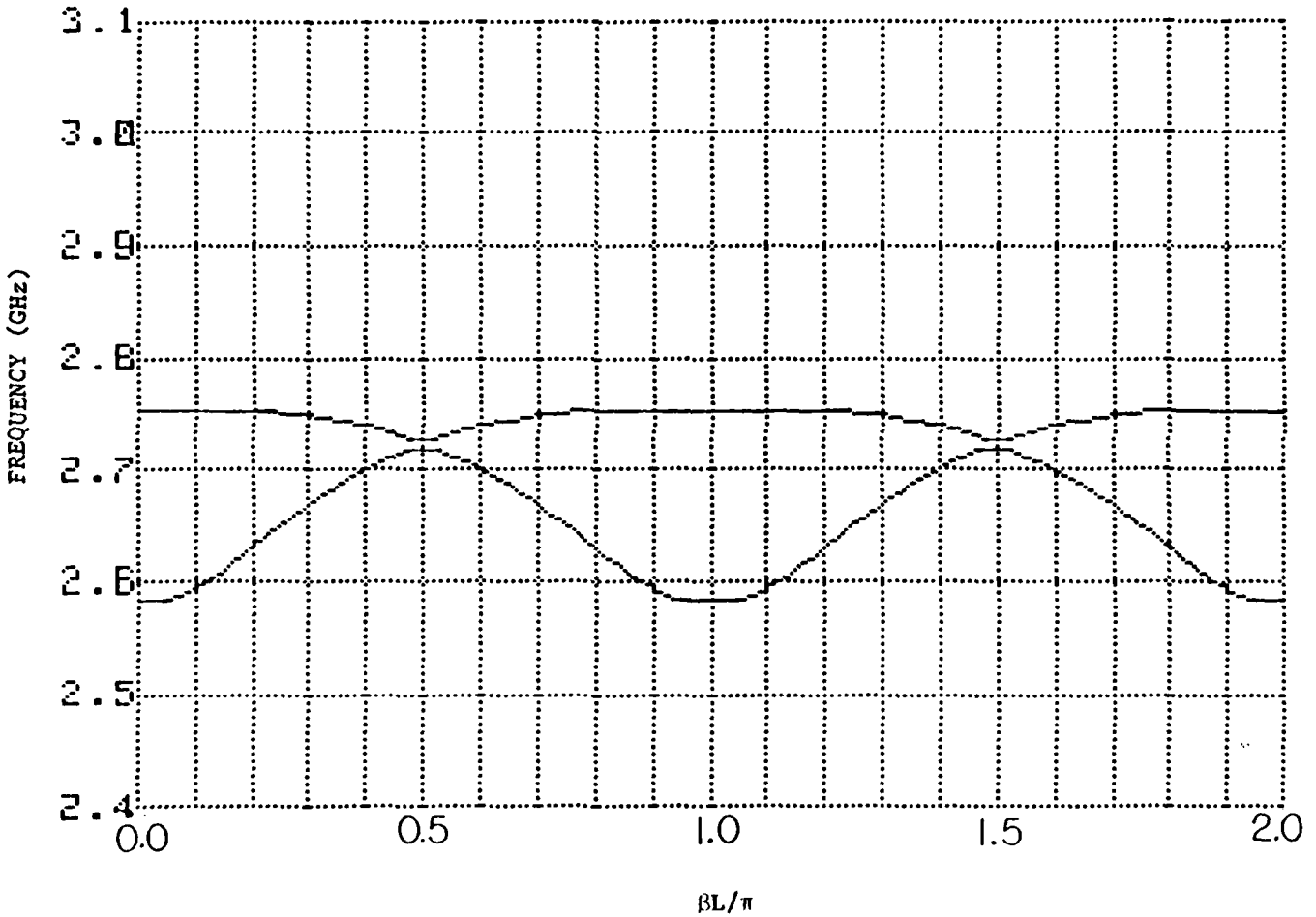

Fig. 14. Brillouin diagram obtained with interface impedance modulation (M = 1.03).

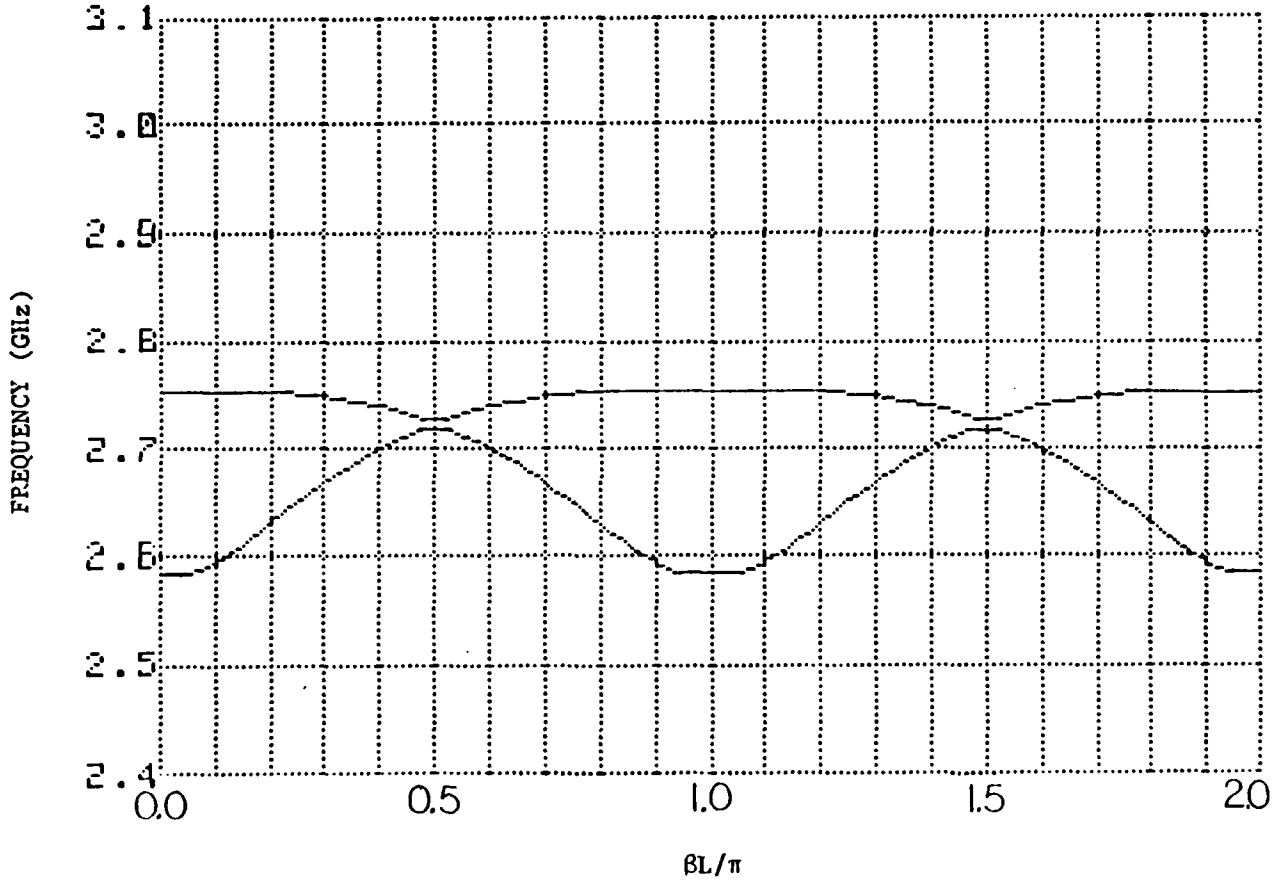

Fig. 15. Interface impedance modulation (M = 1.10).

D. Biperiodic Modulation of Resonator Impedance

Modulating the resonator impedance with M = 1.03 (Fig. 16) produces a narrow stopband in the vicinity of 2.72 GHz. But increasing M to 1.10 provides little change in the ω-β curves. (Figures 16 and 17 differ little even though the corresponding change in the physical structure would be appreciable.) Physically this modulation could be implemented with alternately narrow and wide ladder openings.

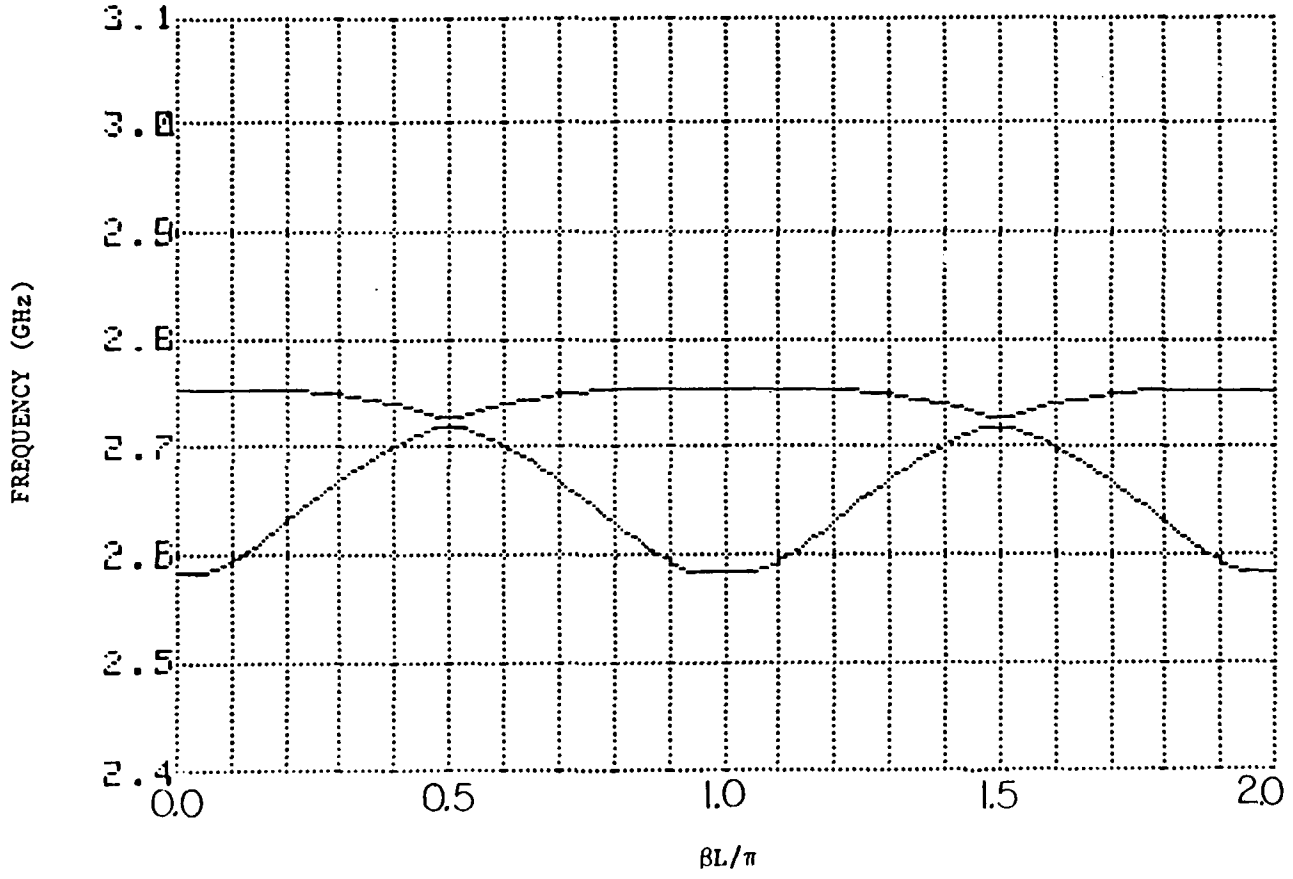

Fig. 16. Brillouin diagram obtained with resonator impedance modulation (M = 1.03).

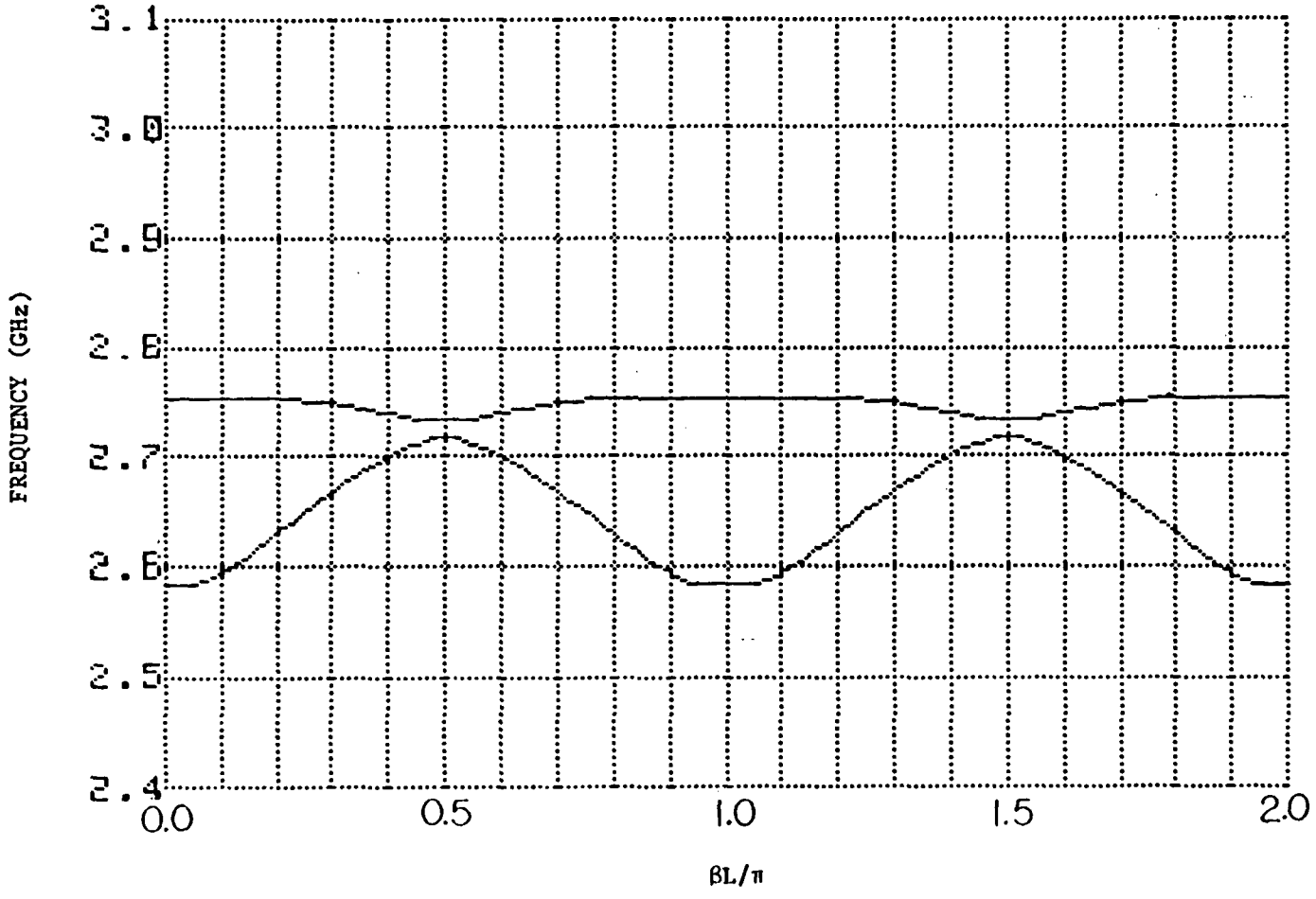

Fig. 17. Resonator impedance modulation (M = 1.10).

E. Biperiodic Modulation of Resonator Frequency

Constrasting with the previous results are the ones due to biperiodic modulation of the resonator frequency. This is the basis of the Varian Canada, Inc. TWT under development. White, Birdsall, and Grow appear to anticipate the current interest in this TWT with their "double" or "stagger-tuned" ladder [10]. A very small modulation (M = 1.01) corresponding physically to ±1 percent of the length of the ladder openings produces effects (Fig. 18) similar to the stronger modulations of the previous cases, but when M is increased slightly to 1.04, the Brillouin diagram of Fig. 19 demonstrates dramatically the effects of passband splitting. The upper ω-β curve has reversed slope, becoming "forward fundamental," and the lower passband is narrower. Further modulation to M = 1.10 (Fig. 20) increases the "cold" bandwidth of the upper passband which exhibits less dispersion than shown in general by the original unmodulated structure (Fig. 12). The lower ω-β curve (Fig. 20) has now reversed slope to become "backward fundamental". With M = 1.14 (Fig. 21) the "cold" bandwidths of both passbands increase (the upper to 9.7 percent). More important than the "cold" bandwidth is the almost constant phase velocity in the higher passband over a wide "hot" bandwidth in the interval $1 < \beta L/\pi < 1.5$, and the flatness at the top of the curve as discussed in connection with Fig. 2c. While the upper passband would be used here for TWT amplification, the lower passband still exists and interaction with the electron beam (at the intersection of the lower ω-β curve with the "beam line") is conceivable. Although beyond the scope of this paper, it can be shown, however, that interference with amplifier operation would not occur for this design.

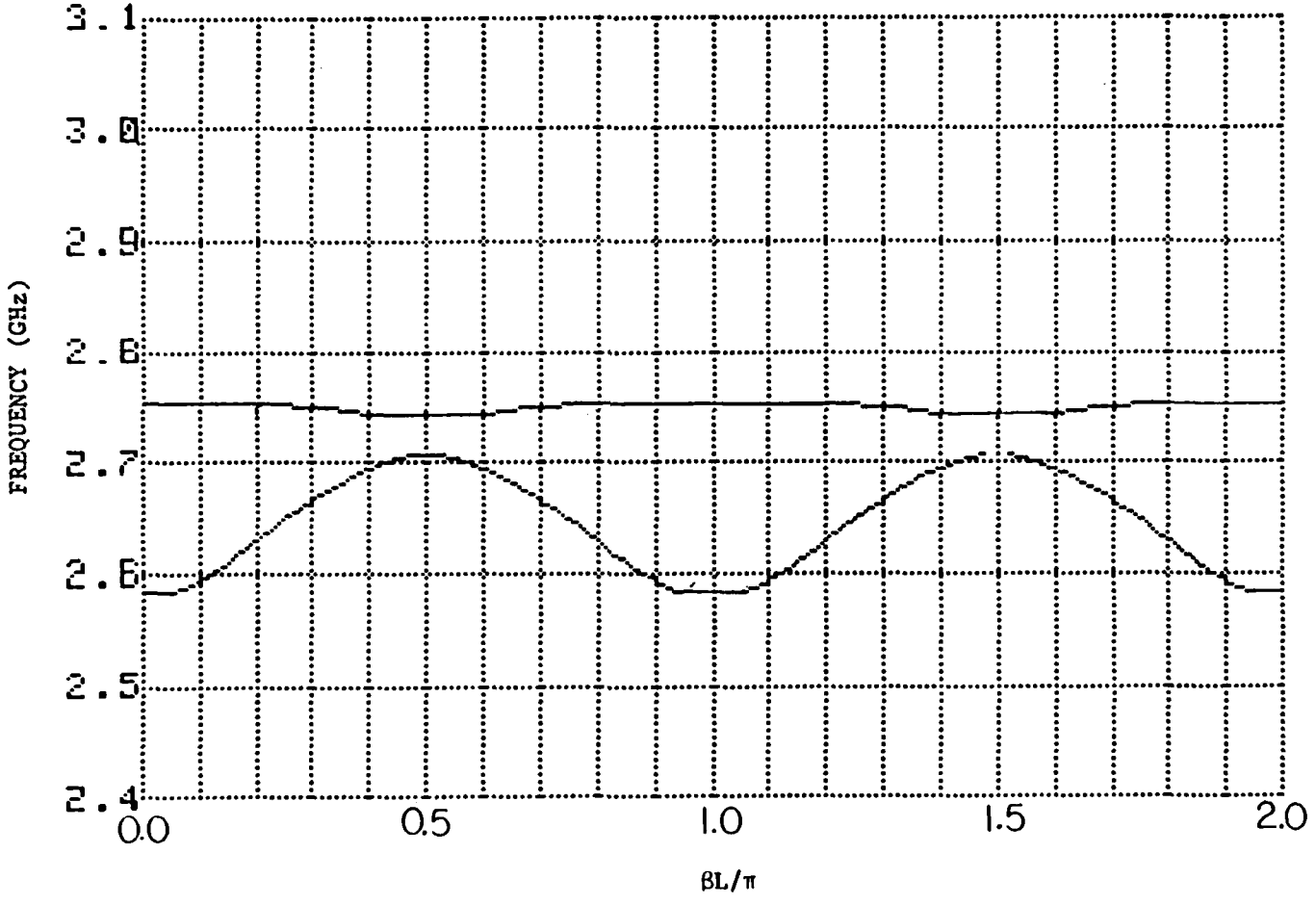

Fig. 18. Brillouin diagram obtained with resonator frequency modulation (M = 1.01).

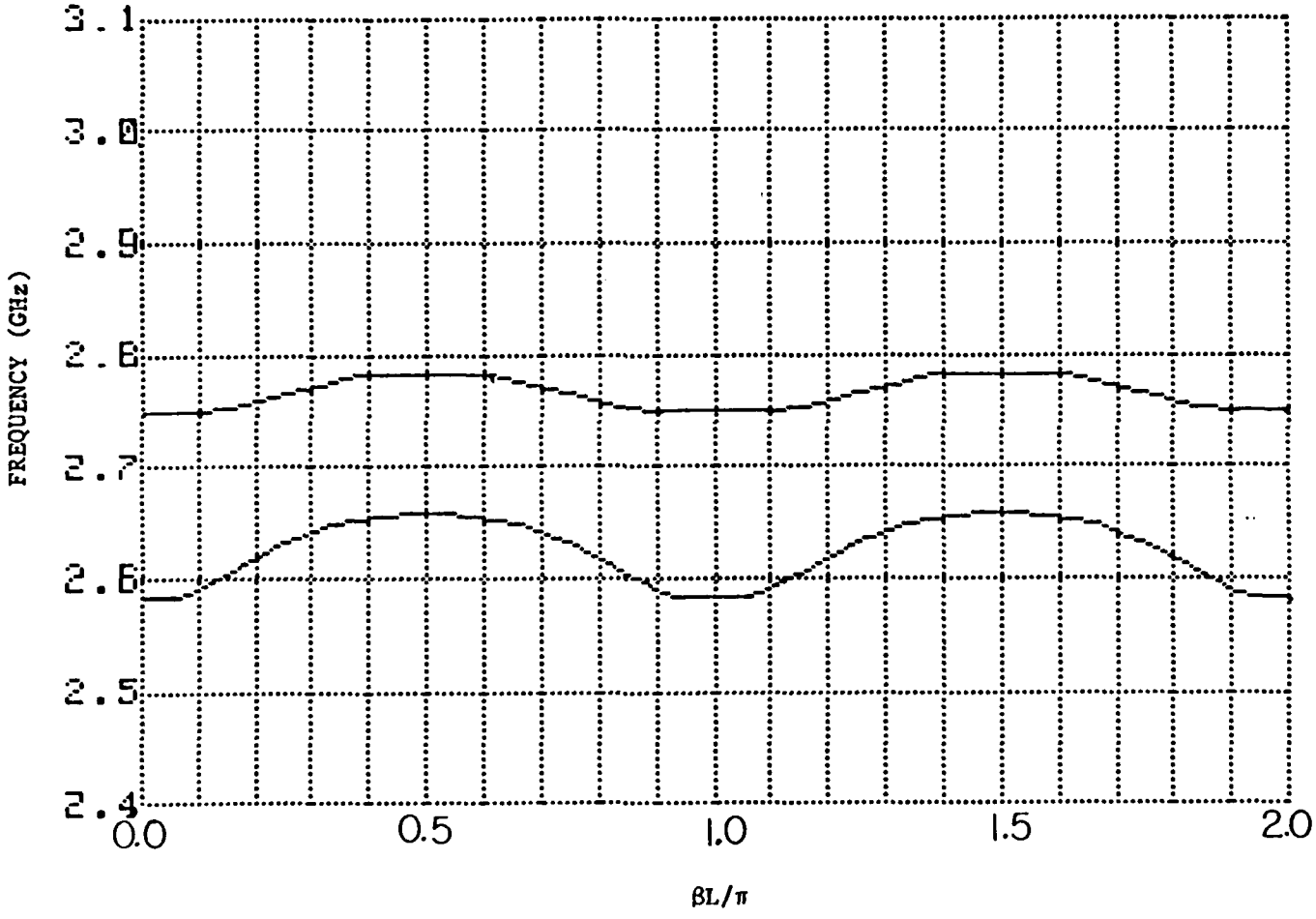

Fig. 19. Resonator frequency modulation (M = 1.04).

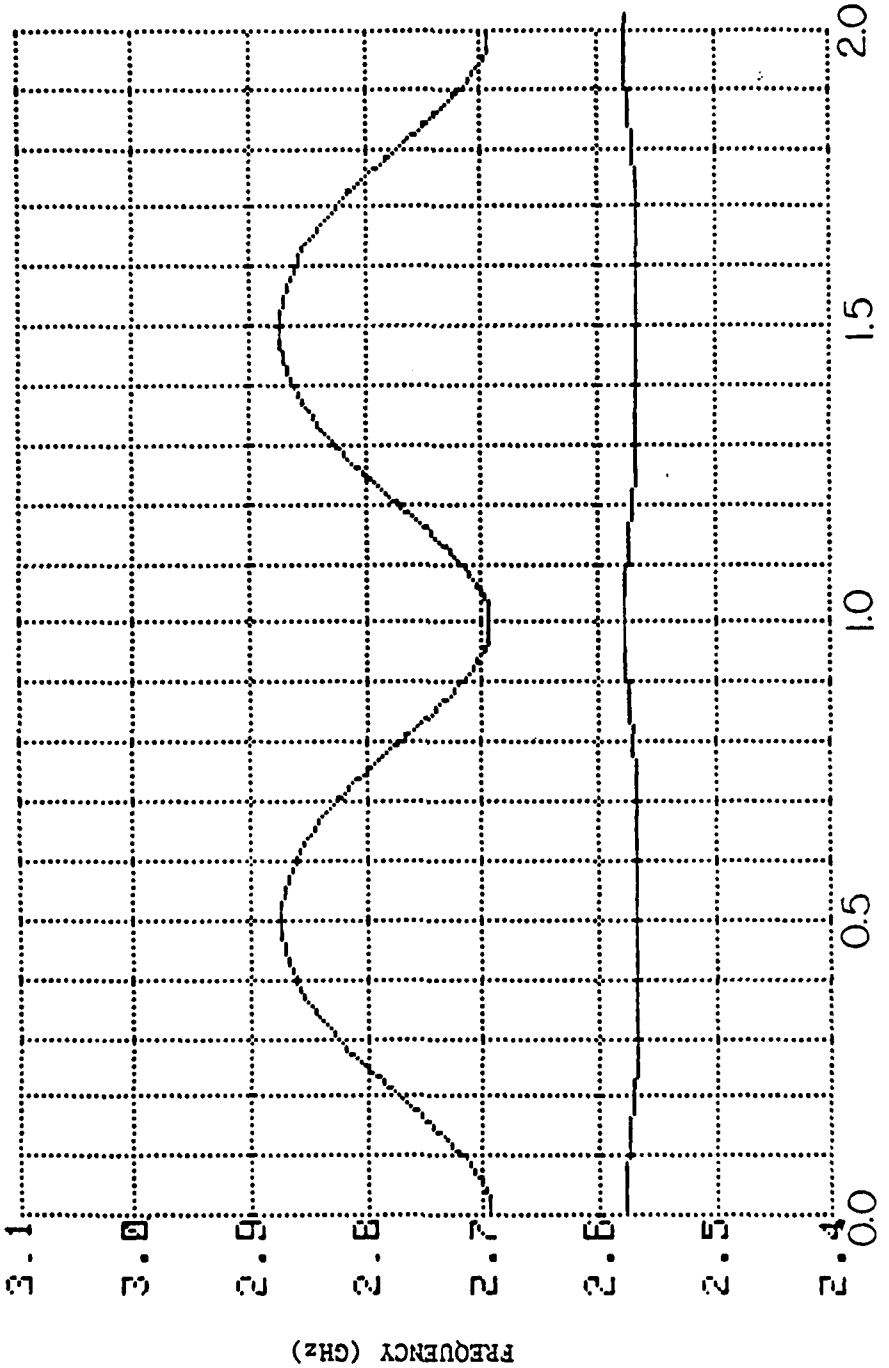

Fig. 20. Resonator frequency modulation (M = 1.10).

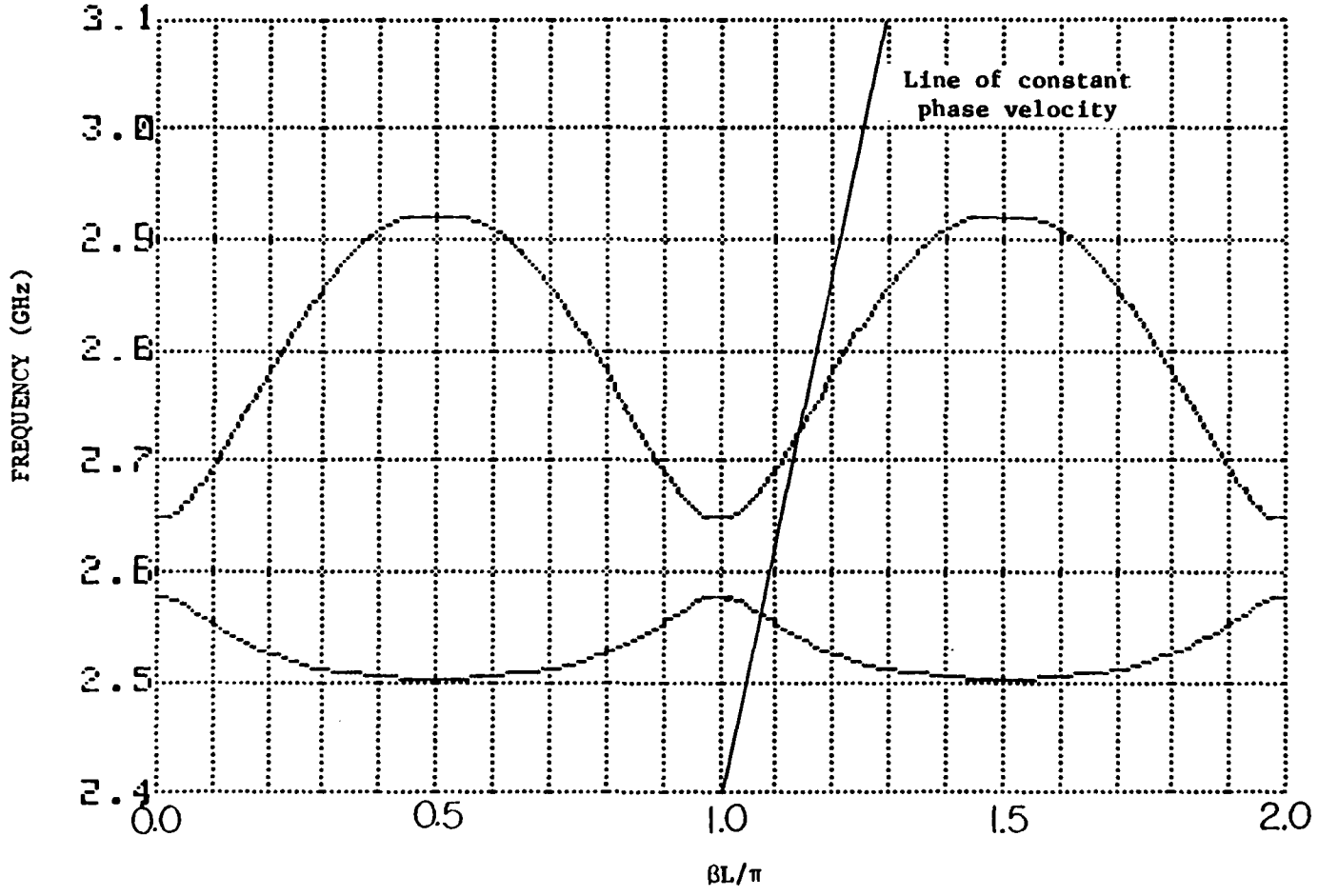

Fig. 21. Resonator frequency modulation (M = 1.14).

F. Combinations of Biperiodic Modulations

The remaining cases of the biperiodic free-ladder structure represent combinations of the four basic biperiodic modulations. These combinations are investigated to assess the possible merit of suggestions that "mixed" modulations might lead to more "hot" bandwidth than would modulation of a single parameter. Figure 22 demonstrates the results of modulating both the interface impedance (M = 1.10) and the resonator frequency (M = 1.14). Comparison with Fig. 21 shows negligible changes due to the additional modulation. Figure 23 shows the Brillouin diagram produced by both interface and resonator frequency modulation. A change from Fig. 21 is apparent, but dispersion is adversely affected. Figures 24 and 25 are the Brillouin diagrams for biperiodic modulation of both resonator frequency and impedance in two possible senses: modulating either in phase (+,+) or out of phase (+,-). Again comparison with Fig. 21 shows that only minor changes result from the additional type of modulation.

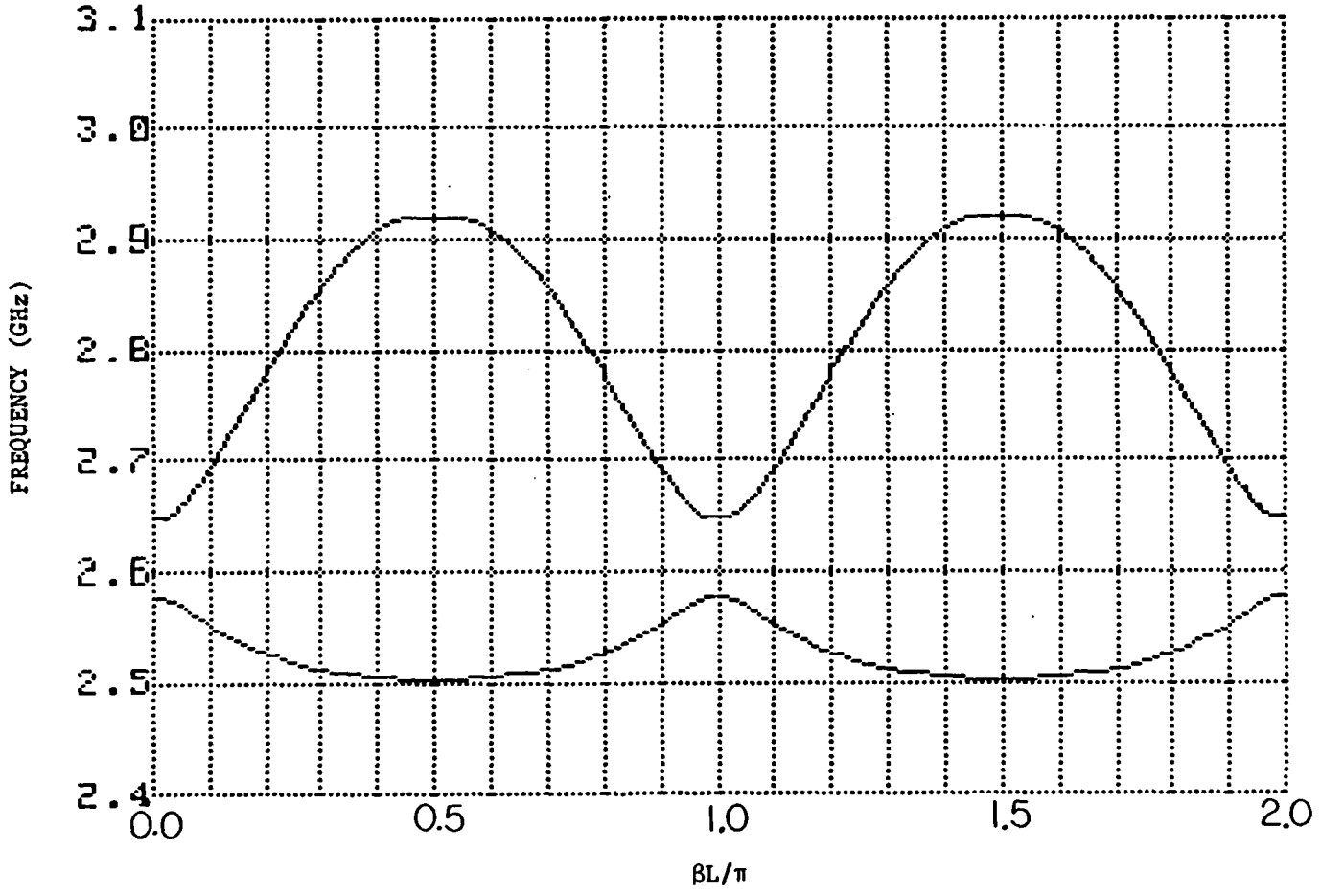

Fig. 22. Brillouin diagram obtained with interface impedance modulation (M = 1.10) and resonator frequency modulation (M = 1.14).

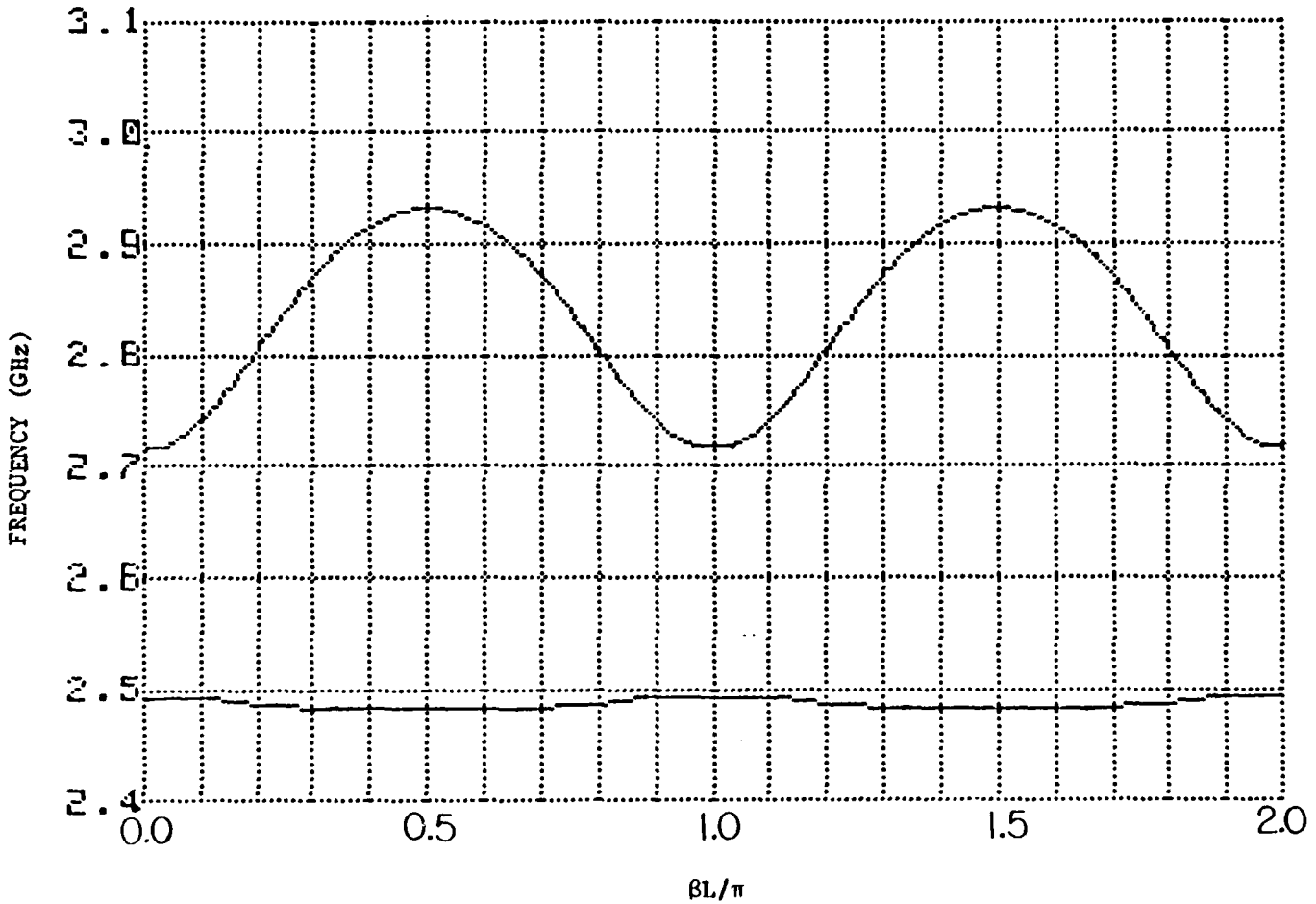

Fig. 23. Brillouin diagram obtained with interface frequency modulation (M = 1.10) and resonator frequency modulation (M = 1.14).

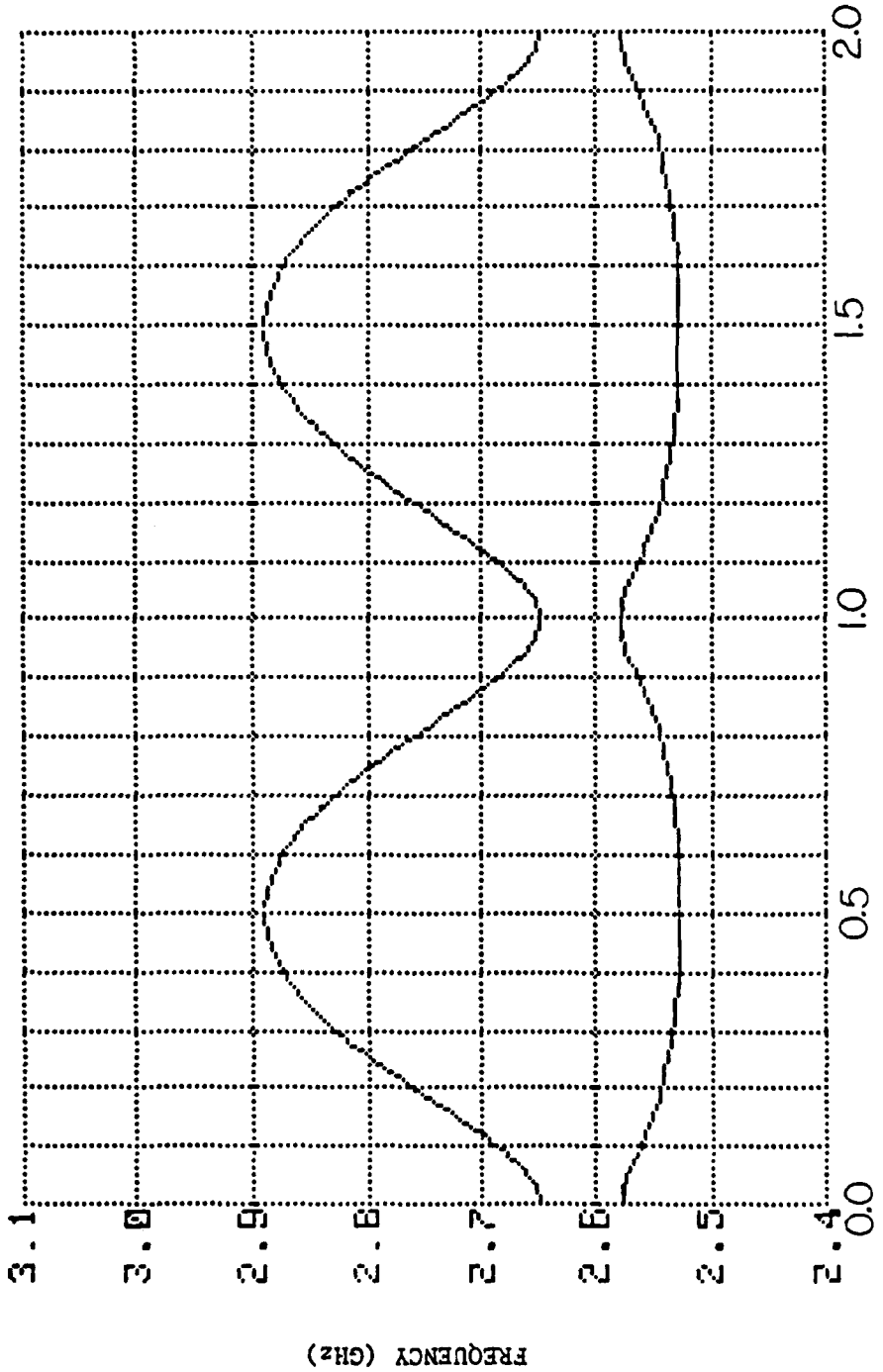

Fig. 24. Brillouin diagram obtained with resonator frequency (+) and impedance (+) modulation (in phase).

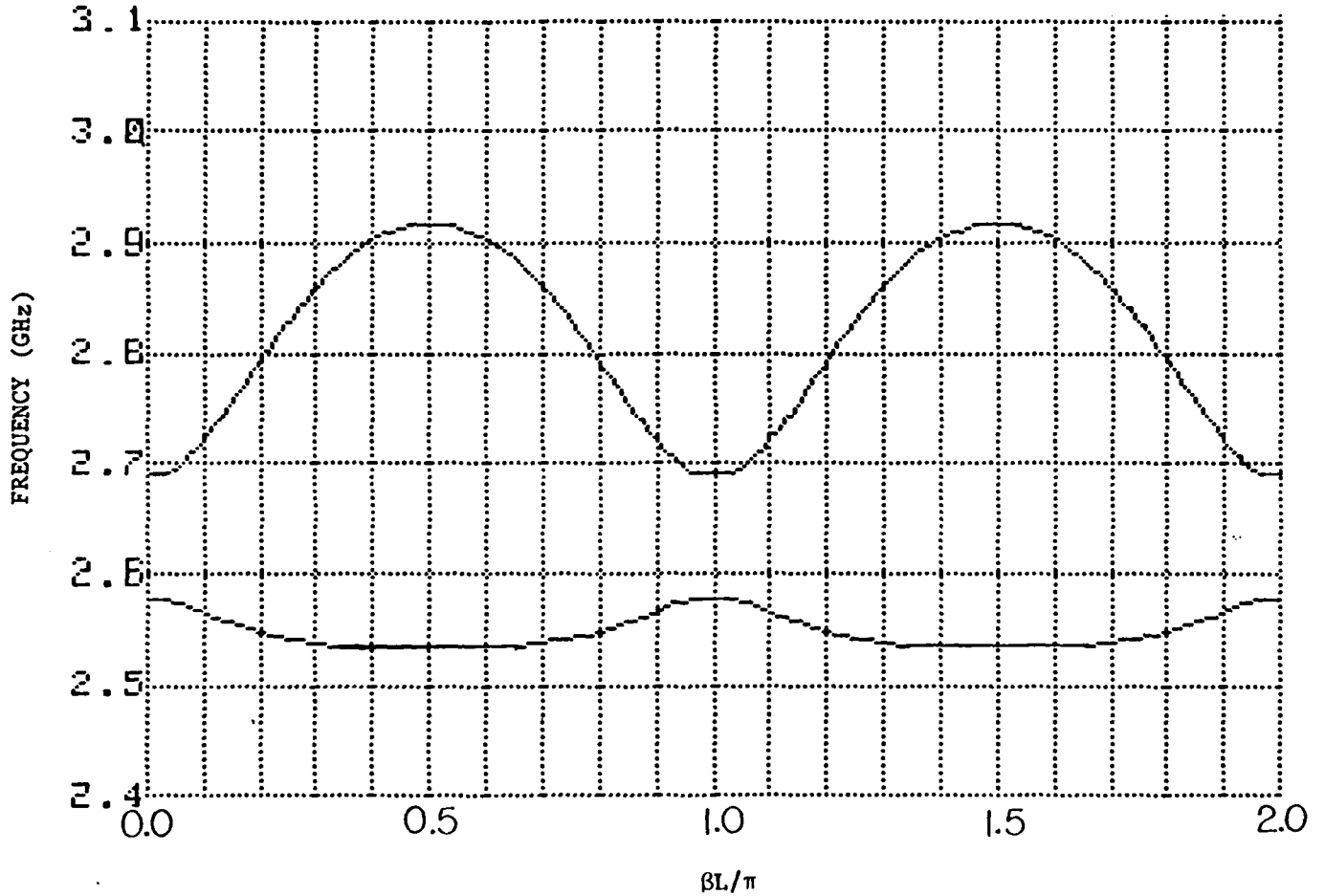

Fig. 25. Brillouin diagram obtained with resonator frequency (+) and impedance (-) modulation (out of phase).

VII. CAVITY CHAIN WITH STAGGERED SINGLE COUPLING SLOT

A. Unmodulated Structure

The next TWT periodic circuit to be studied is the coupled-cavity structure of Fig. 11b. The cavity is circular with a ferrule-less beam hole and with narrow coupling slots staggered in successive coupling interfaces. Prior to introducing biperiodic modulation, the slots subtend an angle of 160°. In the Brillouin diagram of Fig. 26, the lowest passband is seen to be "backward fundamental" with a "cold" bandwidth of 80.5 percent. This geometry is not intended to serve as a CCTWT amplifier, but as a model to which increasing degrees of biperiodic modulation are applied. One possible intent is to find a promising design for a new kind of CCTWT amplifier using biperiodicity to provide bandwidth and stability advantages. Another intent is to gain an understanding of the propagation characteristics of a generic coupled-cavity chain with coupling interfaces with biperiodic variation affecting either the conventional, useful cavity mode (TM°_{010}) or a potentially troublesome higher-order mode (TM°_{110}).

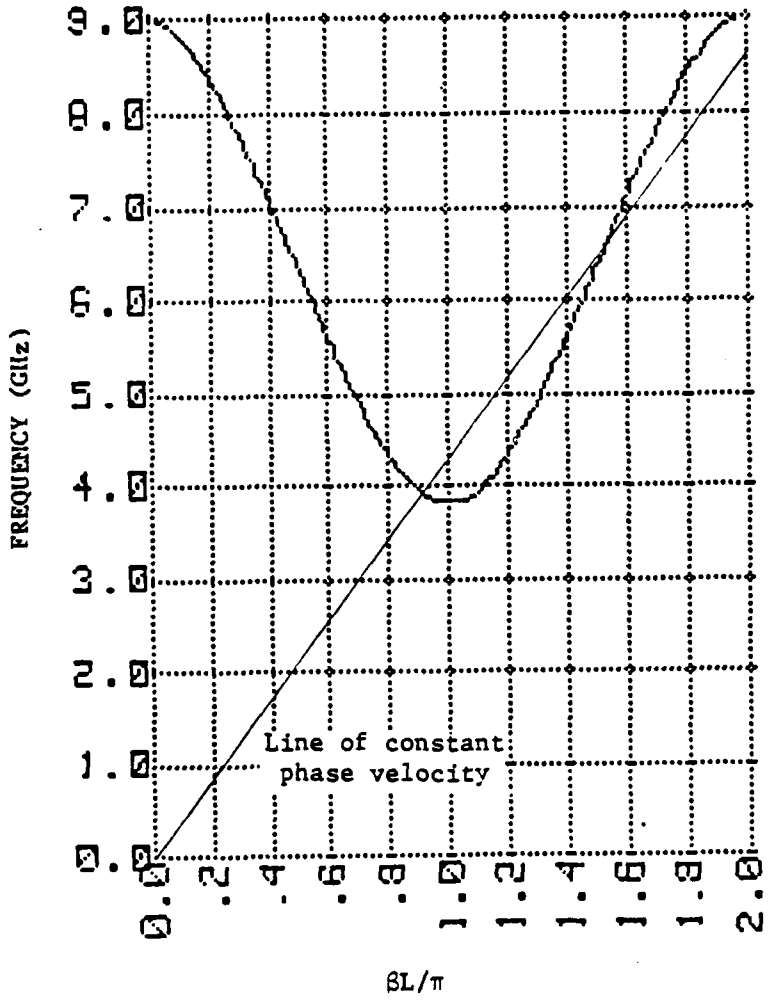

Fig. 26. Brillouin diagram of staggered coupled-cavity structure of Fig. 11b (lowest passband only).

B. Biperiodic Modulation of the Interface Frequency

In the structure of Fig. 11b biperiodic modulation of the interface frequency is introduced by alternately lengthening and shortening the coupling slots, the angle subtended by the slot being α. This is accomplished by multiplying C_3 and L_3 by a modulation factor

$$M = \alpha/160$$

where α is in degrees. The total subtense of two consecutive slots always remains at 320°. For example, if slot A is shortened (Fig. 27) to 150° (M = 0.94), then slot B must be lengthened to 170° (M = 1.06). The values of L_{2A} and L_{2B} must correspondingly be adjusted since their participation in L_C is changed from the original unmodulated case. L_2 is calculated from

$$L_2 = (360/\alpha)\ L_C$$

The values of L_1 and L_9 remain constant since their participation in L_C remains unchanged.

Increasing slot modulation to the point where α_A = 120° (M = 0.75) and α_B = 200° (M = 1.33) produces the Brillouin diagram of Fig. 28, showing the formation of two passbands with a stopband between 5.5 GHz and 7.2 GHz. Note that the extreme lower and upper frequencies (3.8 GHz and 9.0 GHz) are virtually the same as in Fig. 26. The lowermost passband of Fig. 28 (shown with a different vertical scale including the

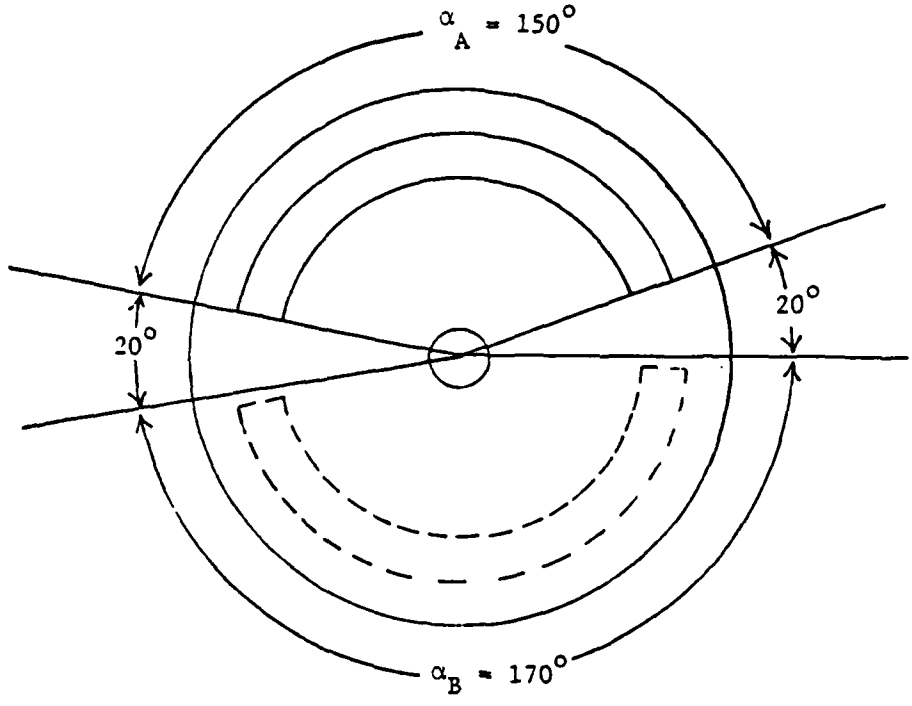

Fig. 27. Interface frequency modulation to $\alpha_A = 150°$ and $\alpha_B = 170°$.

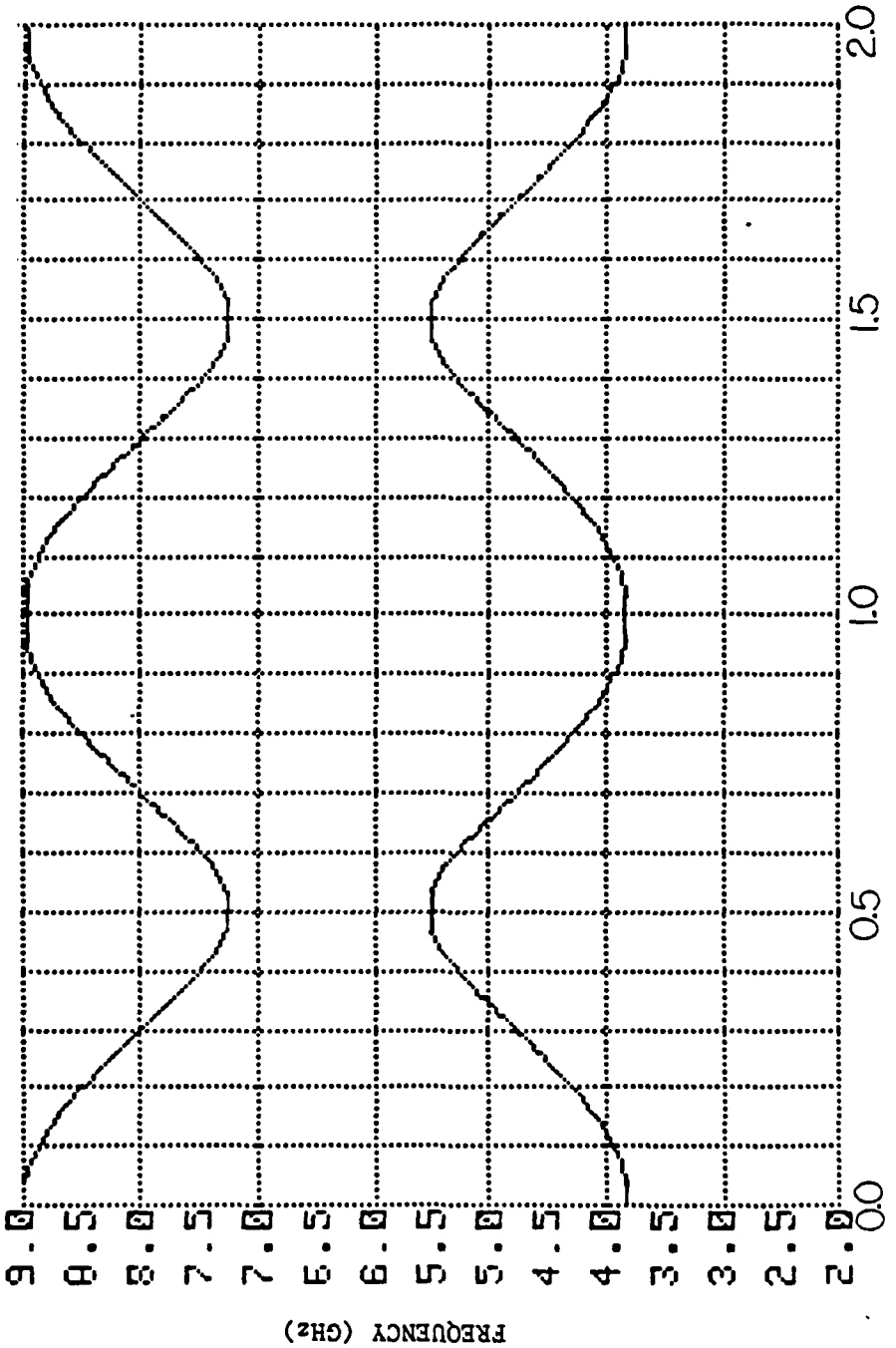

Fig. 28. Brillouin diagram obtained with interface frequency modulation ($\alpha_A = 120°$, $\alpha_B = 200°$).

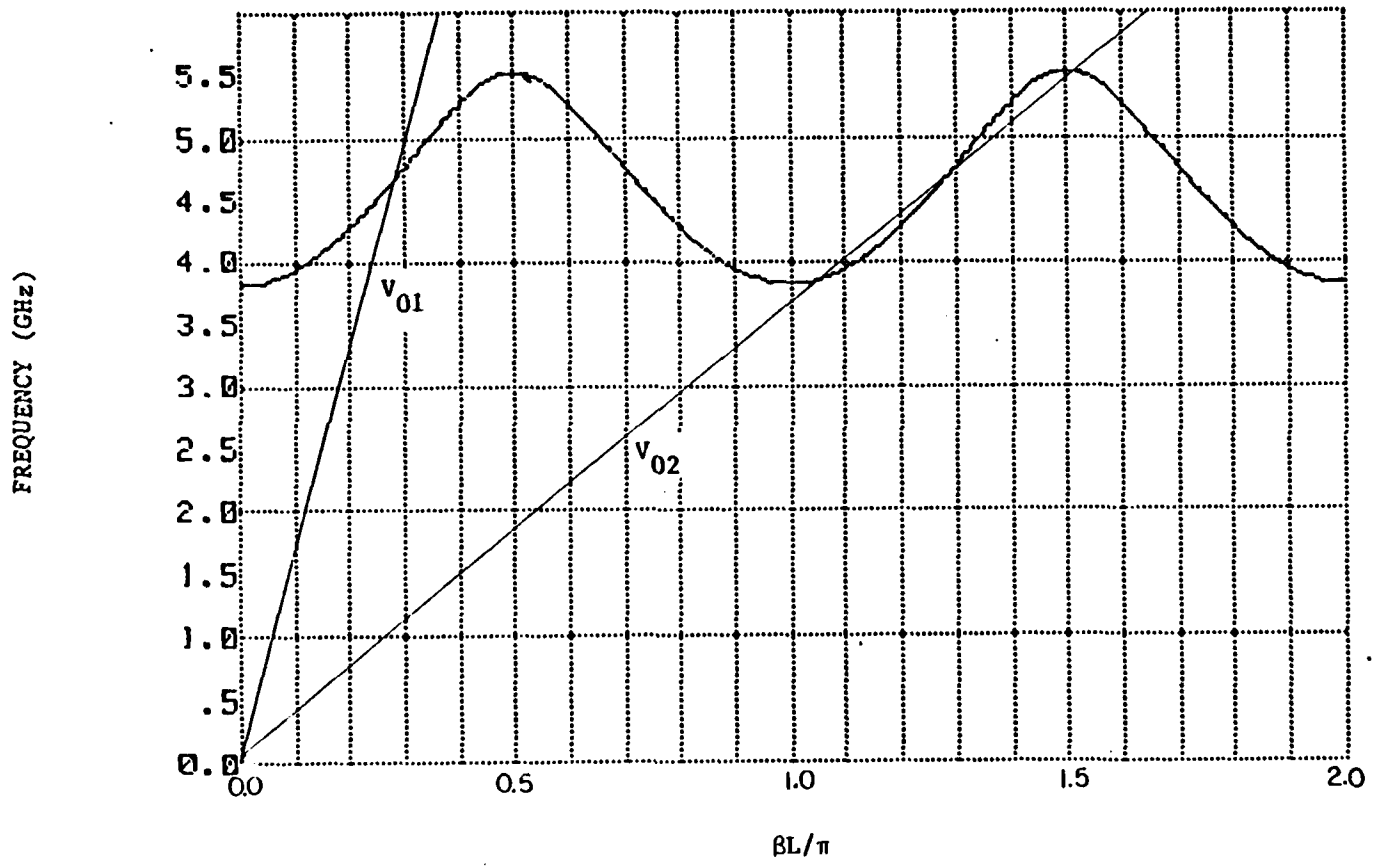

Fig. 29. Lowermost passband of Fig. 28 replotted with different vertical scale.

origin in Fig. 29) is forward fundamental with a "cold" bandwidth of 34.9 percent.

An amplifier could be based on the fundamental interval $0 < \beta L/\pi < 0.5$ (beam line V_{01} in Fig. 29), but the voltage would be impractically high unless the period were made very short. The space-harmonic interval $1 < \beta L/\pi < 1.5$ (beam line V_{02}) could be a practical choice, but the relation of the beam line to the ω-β curve is unsatisfactory (i.e., too many intersections).

The alternating slot angles $\alpha_A = 90°$ ($M = 0.56$) and $\alpha_B = 230°$ ($M = 1.44$) provide the Brillouin diagram of Fig. 30 which shows only the lowest passband. While its "cold" bandwidth has actually decreased, conditions for wide "hot" bandwidth are very promising as seen in how the beam line (V_0) approximates much of the ω-β curve in the $1 < \beta L/\pi < 1.5$ space harmonic-interval.

Stronger biperiodic modulation to $\alpha_A = 70°$ and $\alpha_B = 250°$ ($M = 0.44$ and 1.56), the results of which are plotted in Fig. 31, is seen to be counterproductive since bandwidth potential has become poorer.

In conclusion, a potentially useful new CCTWT design approach has been demonstrated for operation in the space-harmonic interval $1 < \beta L/\pi < 1.5$, with slot angles alternating between 90° and 230° (Fig. 30). In addition, we now have the technique for predicting Brillouin diagrams for any CCTWT structure with modulation of interface frequency, and have learned how its four principal passbands (in terms of phase and group velocities in the various space-harmonic intervals) relate to the two passbands of the unmodulated structure.

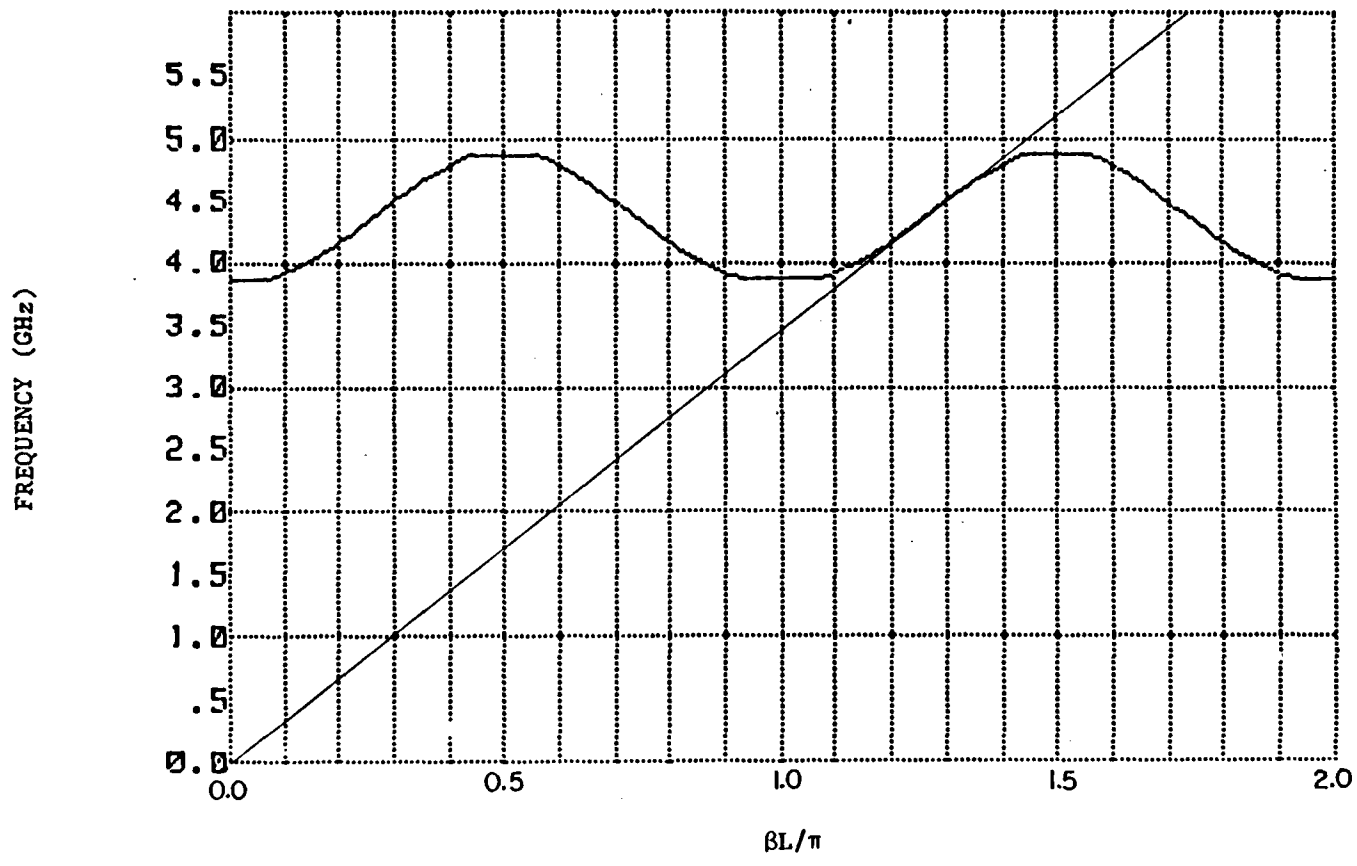

Fig. 30. Interface frequency modulation (α_A = 90°, α_B = 230°).

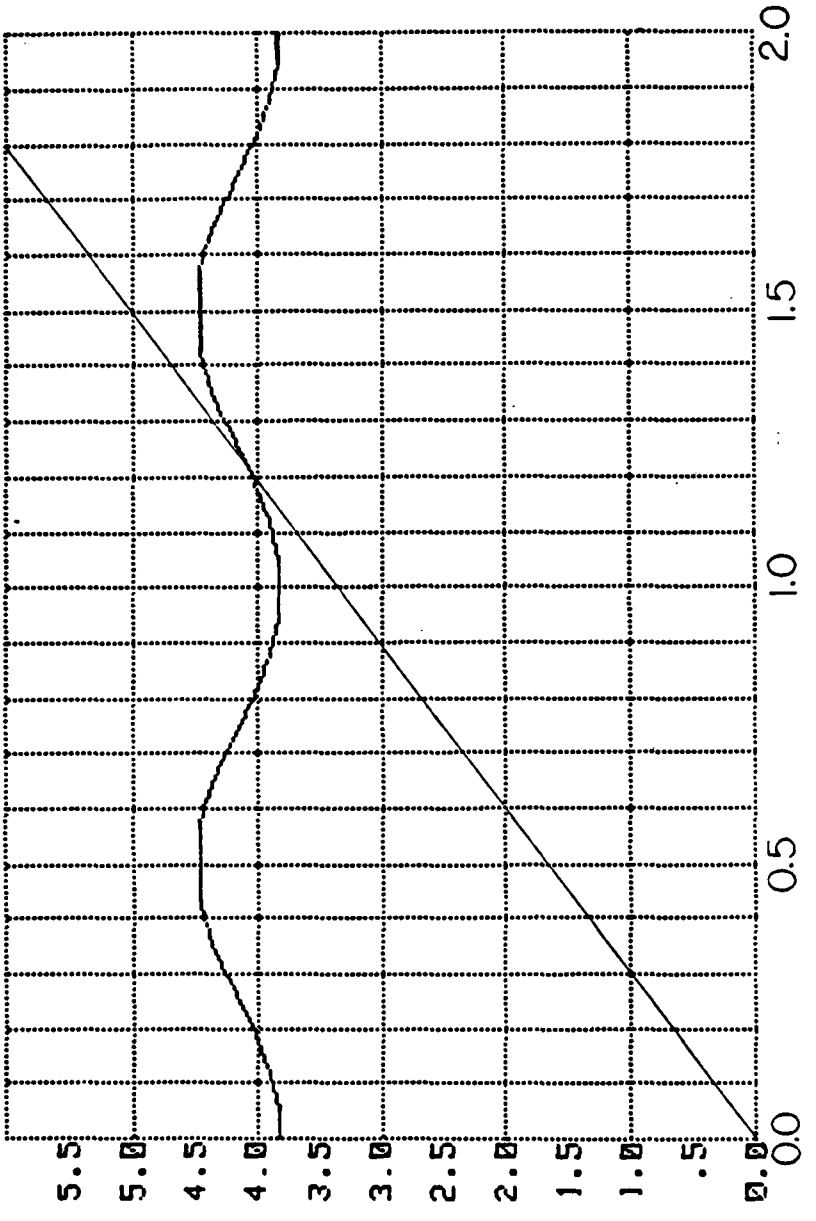

Fig. 31. Interface frequency modulation (α_A = 70°, α_B = 250°).

VIII. RESULTS: CAVITY CHAIN WITH DUAL IN-LINE COUPLING SLOTS

The last TWT periodic structure studied was the coupled-cavity structure of Fig. 32. Since this structure has in-line coupling slots, the L_2 elements in the Curnow cell are very large in relation to the L_1 and L_9 values. In assessing the possible advantages of introducing biperiodicity here, the element values were altered in increments such that the resonator frequency would be modulated by a factor, M. Again each original passband split into two passbands with additional stopbands around frequencies for which $\beta/L = n\pi/2$ (n odd) in the Brillouin diagram of the unmodulated structure. According to the Brillouin diagrams obtained (which are not reproduced here), modulated structures based on an in-line coupled prototype show no promise for a deliberately biperiodic tube.

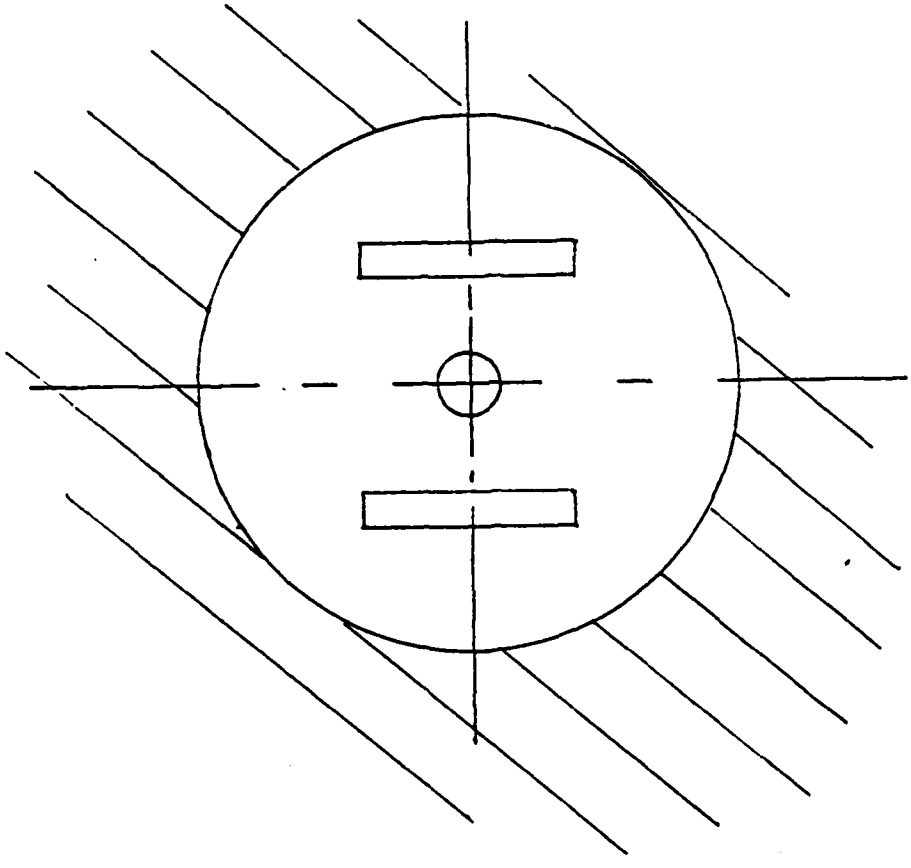

Fig. 32. Dual in-line coupled cavity interaction structure (schematic axial view).

IX. CONCLUSIONS

This research project has established that biperiodic slow-wave structures can be successfully modeled by a sequence of Curnow cells, alternating between two sets of cell parameters. A very convenient procedure has been to start with a sequence of equal cells and then in alternate cells to modulate certain cell element values up and down from the mean.

In the case of the TWT interaction structures whose "biperiodic modulation" is accidental and therefore small, the modeling procedure predicts the narrow stopband where expected. When the procedure was applied to a developmental Varian Canada, Inc. biperiodic TWT, the predicted Brillouin diagram was very close to that measured for the actual tube structure. Applying the procedure to some basic types of generic coupled-cavity interaction structures, the introduction of biperiodicity was produced Brillouin diagrams with characteristics favorable for "hot" bandwidth and stability that could be useful for future TWT designs.

The importance of the biperiodic free-ladder interaction circuit (as used in the Varian Canada, Inc. TWT) made it appropriate to investigate the impact of various forms of biperiodic modulation in extensive detail, a procedure facilitated by the Curnow equivalent-circuit approach. In computer simulation, biperiodic modulations were applied to resonator frequency, resonator impedance, interface frequency, and interface impedance. It was found that only resonator frequency modulation (which happens to be the easiest to implement physically) has an

appreciable advantageous effect on the Brillouin diagram. This type of modulation can lead to a usefully low dispersion and features favorable to stability for a practical tube. The other types of modulation, alone, or combined with resonator frequency modulation, not only increase the physical complexity, but provide no beneficial changes in the "hot"-bandwidth possibilities of the TWT.

Modeling of a representative coupled-cavity structure with side-to-side staggered coupling slots demonstrated the versatility of the procedure developed and illustrated the effects on the Brillouin diagram of biperiodically modulating the interface frequency in this category of structure. In this case it was shown that this form of modulation can provide ω-β curves suitable for practical TWTs even when the unmodulated structure has an unsuitable characteristic.

While certain coupled-cavity TWTs are not biperiodic for the useful mode of propagation, they are effectively biperiodic for some higher-order propagation modes. The developed Curnow equivalent-circuit model can be used to provide Brillouin diagrams to map and understand the higher-order modes with the very practical aim of analyzing and preventing problems in tube operation due to them. One kind of standard coupled-cavity structure (Fig. 5) in particular, effectively has coupling slots that are both spatially staggered and modulated in frequency with respect to a certain higher-order mode of interest. Predicting the Brillouin diagrams for this case in itself was of practical value.

NOTES AND REFERENCES

1. A. Karp, "Biperiodicity as Liability and as Asset in Non-Helix Linear-Beam TWT Interaction Structures," IEDM Technical Digest, Paper 17.2, December 1983, pp. 440-443.

2. A. Hessel, M. H. Chen, R. C. M. Li, A. A. Oliner, "Propagation in Periodically Loaded Waveguides with Higher Symmetries," Proceedings of the IEEE, Vol. 61, No. 2, February 1973, pp. 183-195.

3. Discussion refers to novel "biperiodic free ladder" millimeter-wave TWTs under development by Varian Canada, Inc. in Georgetown, Ontario.

4. B. Arfin, "A Traveling-Wave Tube Using Coupled Coaxial Cavities," Technical Report No. 220-1, Stanford Electronics Laboratories and Microwave Laboratory, Stanford University, Stanford, California, October 30, 1956.

5. F. Friedlander et al., "Transient Analysis of Beam Interaction with Antisymmetric Mode in Truncated Periodic Structure using 3-Dimensional Computer Code SOS," scheduled for publication, IEDM Technical Digest, December 1985.

6. H. J. Curnow, "A General Equivalent Circuit for Coupled-Cavity Slow-Wave Structures," IEEE Transactions on Microwave Theory and Techniques, Vol. MTT-13, 1965, pp. 671-675.

7. S. P. Darbin, "Synthesis of Microwave SLow-Wave Structures from Lumped-Element Equivalents," Stanford AFTER Thesis, August 1982.

8. D. B. Aster, Varian Associates, Inc., Palo Alto, California, unpublished network-analysis computer programs, derivations, and documentation.

9. P. J. Crepeau and P. R. McIsaac, "Consequences of Symmetry in Periodic Structures," Proceedings of the IEEE, Vol. 52, January 1964, pp. 33-43.

10. R. M. White, C. K. Birdsall, R. W. Grow, "Multiple Ladder Circuits for Millimeter-Wavelength Traveling-Wave Tubes," Symposium on Millimeter Waves, Polytechnic Institute of Brooklyn, April 1959, pp. 367-402.

APPENDIX A. A SAMPLE CALCULATION OF CURNOW VALUES

These calculations pertain to the geometry depicted in Fig. 11b. Given a circular-format cavity with a resonance frequency F_C = 9 GHz and R/Q = 30 ohms, C_1 and L_C can be calculated from A.1 and A.2.

$$F_C = (4\pi^2 C_1 L_C)^{-1/2} \tag{A.1}$$

$$R/Q = (L_C/C_1)^{1/2} \tag{A.2}$$

$$C_1 = .58946 \text{ pF}$$

$$L_C = .53052 \text{ nH}$$

To evaluate the individual inductors comprising L_C, with regard to the coupling slots of Fig. 11b, the fractions m, p, n, for each constituent inductor must be approximated. For a first approximation the radial RF cavity currents are assumed to be distributed uniformly in azimuth about the beam hole. Thus

$$p = \pi/(\pi - \psi)$$

and

$$m = 2\pi/\psi$$

where ψ is the angle subtended by a particular coupling slot. The fraction 1/p of the total current can circulate to the opposite cavity face without crossing a coupling slot. The fractions crossing only one coupling slot are $1/m_A$ and $1/m_B$. From the above fractions

$$L_1 = pL_C$$

$$L_{2A} = m_A L_C$$

$$L_{2B} = m_B L_C$$

$$L_1 = 4.7749 \text{ nH}$$

$$L_{2A} = L_{2B} = 1.1937 \text{ nH}.$$

When $\psi < \pi$, L_9 can be chosen very large in relation to the other values: $L_9 = 500$ nH.

For the remaining two elements, L_3 and C_3, use is made of

$$F_s = \text{slot frequency} = (4\pi^2 C_3 L_3)^{-1/2} \qquad \text{(A.3)}$$

and

$$Z_s = \text{slot impedance} = (L_3/C_3)^{1/2}. \qquad \text{(A.4)}$$

The slot impedance is estimated to be 100 ohms. The cavity radius, 1.27 cm, can be estimated from the cavity frequency, 9 GHz, assuming no "ferrule" around the beam hole. From the slot and cavity geometry, and the angle $\psi = 160°$, an effective slot length of 3 cm may be estimated, yielding a slot frequency of 5 GHz, at which this slot would be half-wave resonant. Then, from Eqs. A.3 and A.4,

$$C_3 = .31831 \text{ pF}$$

and

$$L_3 = 3.1831 \text{ nH}.$$

APPENDIX B. CALCULATION OF BETA

With reference to the two circuit cells of Fig. B1, the final, desired result is a matrix relating the output voltage and current to the input voltage and current. From Fig. B1 this would be

$$\lambda \begin{bmatrix} V_0 \\ I_0 \end{bmatrix} = \begin{bmatrix} V_5 \\ I_5 \end{bmatrix} = \begin{bmatrix} A & B \\ C & D \end{bmatrix} \begin{bmatrix} V_0 \\ I_0 \end{bmatrix}$$

To reach this result, a series of transmission-line sections must be cascaded together relating the intermediate voltages and currents shown in Fig. B1.

$$\begin{bmatrix} V_1 \\ I_1 \end{bmatrix} = \begin{bmatrix} A_0 & B_0 \\ C_0 & D_0 \end{bmatrix} \begin{bmatrix} V_0 \\ I_0 \end{bmatrix} \tag{B.1}$$

$$\begin{bmatrix} V_2 \\ I_2 \end{bmatrix} = \begin{bmatrix} A_1 & B_1 \\ C_1 & D_1 \end{bmatrix} \begin{bmatrix} V_1 \\ I_1 \end{bmatrix} \tag{B.2}$$

$$\begin{bmatrix} V_3 \\ I_3 \end{bmatrix} = \begin{bmatrix} A_2 & B_2 \\ C_2 & D_2 \end{bmatrix} \begin{bmatrix} V_2 \\ I_2 \end{bmatrix} \tag{B.3}$$

$$\begin{bmatrix} V_4 \\ I_4 \end{bmatrix} = \begin{bmatrix} A_3 & B_3 \\ C_3 & D_3 \end{bmatrix} \begin{bmatrix} V_3 \\ I_3 \end{bmatrix} \tag{B.4}$$

$$\begin{bmatrix} V_5 \\ I_5 \end{bmatrix} = \begin{bmatrix} A_4 & B_4 \\ C_4 & D_4 \end{bmatrix} \begin{bmatrix} V_4 \\ I_4 \end{bmatrix} \tag{B.5}$$

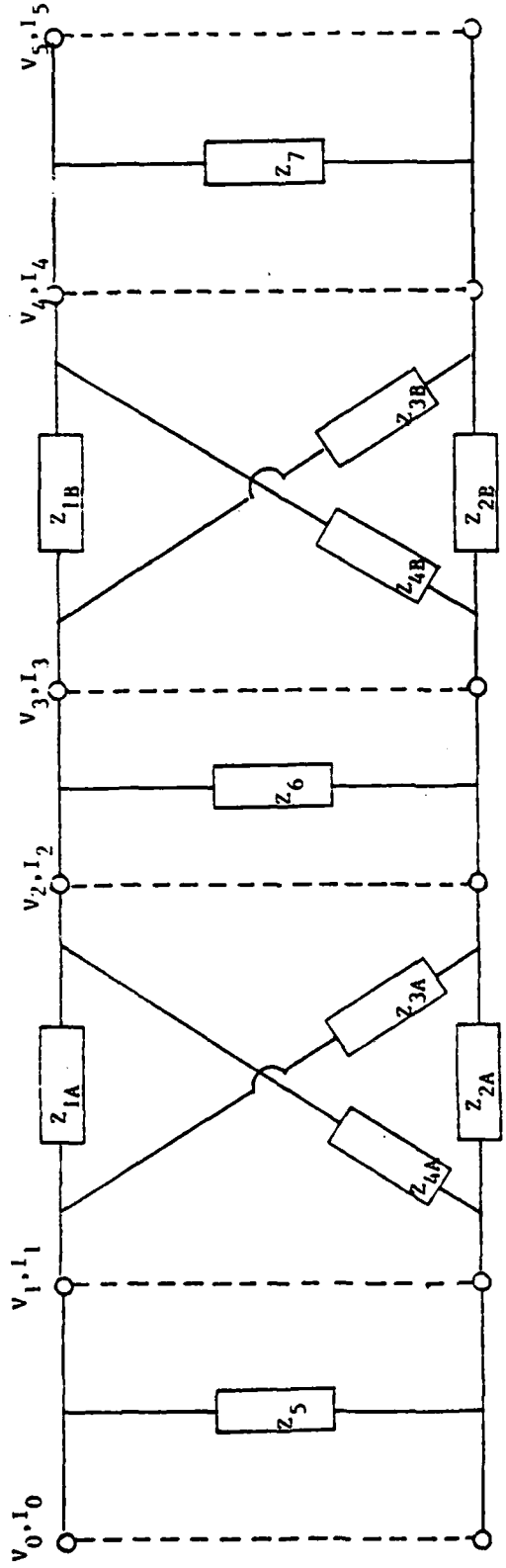

Fig. B1. Curnow cells separated into transmission-line sections.

Shunt impedances are represented by matrices B.1, B.3, and B.5 and may be written

$$\begin{bmatrix} V_n \\ I_n \end{bmatrix} = \begin{bmatrix} 1 & 0 \\ Y_{SHUNT} & 1 \end{bmatrix} \begin{bmatrix} V_{n-1} \\ I_{n-1} \end{bmatrix} \tag{B.6}$$

Matrices B.2 and B.4 refer to resonator equivalent circuits which may be represented generically by Fig. B.2, for which one may write:

$$I_2 = i_1 + i_4 = i_2 - i_3 \tag{B.7}$$

$$V_2 = i_4 Z_4 + i_2 Z_2 = -i_3 Z_3 + i_1 Z_1 \tag{B.8}$$

$$I_1 = i_1 + i_3 = i_2 - i_4 \tag{B.9}$$

$$V_1 = -i_1 Z_1 + i_4 Z_4 = -i_3 Z_3 = i_2 Z_2 \tag{B.10}$$

Rewriting Eq. B.9 as

$$i_1 = I_1 - i_3,$$

and combining with Eq. B.7

$$I_2 = I_1 - i_3 + i_4, \tag{B.11}$$

Rewriting Eq. B.10 as

$$i_3 = (-i_2 Z_2 - V_1)/Z_3 \tag{B.12}$$

and Eq. B.9 as

$$i_2 = I_1 + i_4 \tag{B.13}$$

and combining with Eq. B.12 gives

$$i_3 = \left(-(I_1 + i_4)\, Z_2 - V_1\right)/Z_3.$$

This combined with Eq. B.11 gives

$$I_2 = I_1 + \frac{i_4 Z_2}{Z_3} + \frac{I_1 Z_2}{Z_3} + \frac{V_1}{Z_3} + i_4$$

or

$$I_2 = I_1 \frac{(Z_3 + Z_2)}{Z_3} + \frac{V_1}{Z_3} + i_4 \frac{(Z_3 + Z_2)}{Z_3}. \tag{B.14}$$

Starting with Eq. B.8 and combining with Eq. B.13 gives

$$V_2 = i_4(Z_4 + Z_2) + I_1 Z_2$$

or

$$i_4 = (V_2 + I_1 Z_2)/(Z_4 + Z_2). \tag{B.15}$$

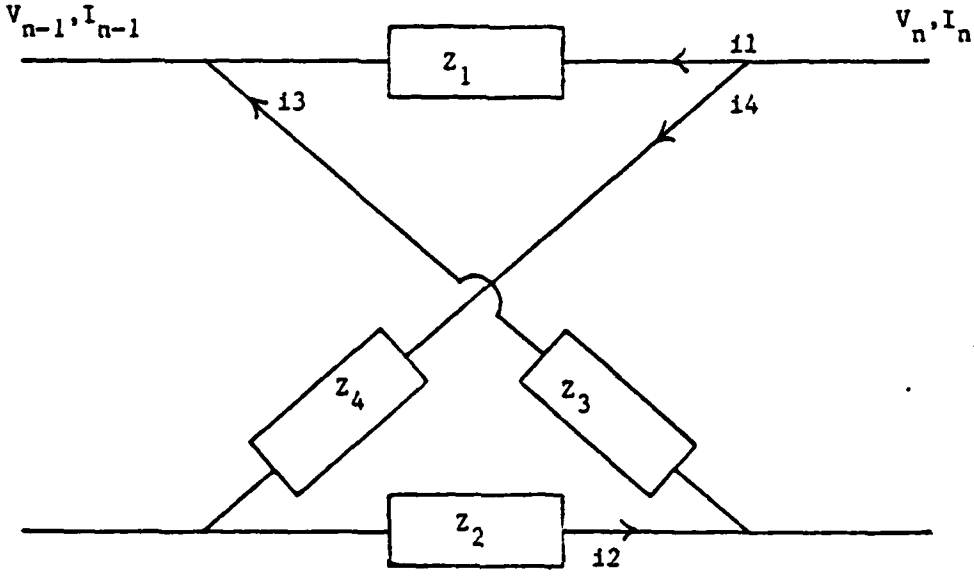

Fig. B2. Transmission-line section for one resonator.

Combining Eq. B.15 with Eq. B.14 gives

$$I_2 = I_1 \frac{(Z_3 + Z_2)}{Z_3} + \frac{V_1}{Z_3} + \frac{V_1(Z_3 + Z_2)}{Z_3(Z_1 + Z_4)} + \frac{I_2 Z_1(Z_3 + Z_2)}{Z_3(Z_1 + Z_4)}$$

or

$$I_2 = \frac{I_1(Z_3 + Z_2)(Z_1 + Z_4)}{Z_3Z_4 - Z_1Z_2} + \frac{V_1(Z_1 + Z_2 + Z_3 + Z_4)}{Z_3Z_4 - Z_1Z_2}. \qquad (B.16)$$

Combining Eqs. B.13 and B.8 gives

$$V_2 = i_4Z_4 + (I_1 + i_4)\, Z_2.$$

Combining this with Eq. B.15 gives

$$V_2 = I_1Z_2 + \frac{V_1(Z_2 + Z_4)}{(Z_1 + Z_4)} + \frac{I_2Z_1\,(Z_2 + Z_4)}{(Z_1 + Z_4)}.$$

Combining this with Eq. B.16 gives

$$V_2 = I_1\left[Z_2 + \frac{Z_1(Z_2+Z_4)(Z_3+Z_2)}{Z_3Z_4 - Z_1Z_2}\right] + V_1\left[\frac{(Z_2+Z_4)}{(Z_1+Z_4)} + \frac{Z_1(Z_2+Z_4)(Z_1+Z_2+Z_3+Z_4)}{(Z_1+Z_4)(Z_3Z_4-Z_1Z_2)}\right].$$

(B.17)

Writing Eq. B.16 and B.17 in matrix form gives

$$\begin{bmatrix} V_2 \\ \\ I_2 \end{bmatrix} = \begin{bmatrix} \dfrac{(Z_2+Z_4)}{(Z_1+Z_4)} + \dfrac{Z_1(Z_2+Z_4)(Z_1+Z_2+Z_3+Z_4)}{(Z_1+Z_4)(Z_3Z_4-Z_1Z_2)} & Z_2 + \dfrac{Z_1(Z_2+Z_4)(Z_3+Z_2)}{Z_3Z_4 - Z_1Z_2} \\ \\ \dfrac{Z_1+Z_2+Z_3+Z_4}{Z_3Z_4 - Z_1Z_2} & \dfrac{(Z_3+Z_2)(Z_1+Z_4)}{Z_3Z_4 - Z_1Z_2} \end{bmatrix} \begin{bmatrix} V_1 \\ \\ I_1 \end{bmatrix}.$$

From Eq. B.18 the values of A, B, C, and D in Matrix B.2 and A, B, C, and D in Matrix B.4 are

$$A_1,\ A_3 = \frac{Z_2 + Z_4}{Z_1 + Z_4} + \frac{Z_1\ (Z_2 + Z_4)(Z_1 + Z_2 + Z_3 + Z_4}{(Z_1 + Z_4)(Z_3Z_4 - Z_1Z_2)}$$

$$B_1,\ B_3 = Z_2 + \frac{Z_1\ (Z_2 + Z_4)\ Z_3 + Z_4}{Z_3Z_4 - Z_1Z_2}$$

$$C_1,\ C_3 = \frac{Z_1 + Z_2 + Z_3 + Z_4}{Z_3Z_4 - Z_1Z_2}$$

$$D_1,\ D_3 = \frac{(Z_3 + Z_2)(Z_1 + Z_4)}{Z_3Z_4 - Z_1Z_2}$$

with

$$Z_1 = (j\omega L_{1A})/(1 - \omega^2\ L_{1A}C_{1A})$$
$$Z_2 = j\omega L_{9A}$$
$$Z_3 = j\omega L_{2B}$$
$$Z_4 = j\omega L_{2A}$$

in Matrix B.2 and with

$$Z_1 = (j\omega L_{1B})/(1 - \omega^2\ L_{1B}C_{1B})$$
$$Z_2 = j\omega L_{9B}$$
$$Z_3 = j\omega L_{2A}$$
$$Z_4 = j\omega L_{2B}$$

in Matrix B.4. Combining Matrix B.6 with Matrices B.1, B.3, and B.5, and cascading them with Matrices B.2 and B.4 gives

$$\lambda \begin{bmatrix} V_0 \\ I_0 \end{bmatrix} = \begin{bmatrix} V_5 \\ I_5 \end{bmatrix} = \begin{bmatrix} 1 & 0 \\ Y_7 & 1 \end{bmatrix} \begin{bmatrix} A_3 & B_3 \\ C_3 & D_3 \end{bmatrix} \begin{bmatrix} 1 & 0 \\ Y_6 & 1 \end{bmatrix} \begin{bmatrix} A_1 & B_1 \\ C_1 & D_1 \end{bmatrix} \begin{bmatrix} 1 & 0 \\ Y_5 & 1 \end{bmatrix} \begin{bmatrix} V_0 \\ I_0 \end{bmatrix}$$

or

$$\lambda \begin{bmatrix} V_0 \\ I_0 \end{bmatrix} = \begin{bmatrix} A_{TOT} & B_{TOT} \\ C_{TOT} & D_{TOT} \end{bmatrix} \begin{bmatrix} V_0 \\ I_0 \end{bmatrix}$$

or

$$\begin{bmatrix} 0 \\ 0 \end{bmatrix} = \begin{bmatrix} A_{TOT} - \lambda & B_{TOT} \\ C_{TOT} & D_{TOT} - \lambda \end{bmatrix} \begin{bmatrix} V_0 \\ I_0 \end{bmatrix}.$$

Since the determinant of the matrix must equal zero,

$$A_{TOT}D_{TOT} - (A_{TOT} + D_{TOT})\,\lambda + \lambda^2 - B_{TOT}\,C_{TOT} = 0 \qquad (B.19)$$

and since, from reciprocity,

$$A_{TOT}\,D_{TOT} - B_{TOT}\,C_{TOT} = 1,$$

Eq. B.19 is

$$\lambda^2 - (A_{TOT}\ D_{TOT})\ \lambda + 1 = 0$$

or

$$\lambda = \frac{A_{TOT} + D_{TOT}}{2} \pm \left[\left(\frac{A_{TOT} + D_{TOT}}{2}\right)^2 - 1\right]^{1/2}.$$

The phase of λ then provides β for a given ω.

MISSION
of
Rome Air Development Center

RADC plans and executes research, development, test and selected acquisition programs in support of Command, Control, Communications and Intelligence (C^3I) activities. Technical and engineering support within areas of competence is provided to ESD Program Offices (POs) and other ESD elements to perform effective acquisition of C^3I systems. The areas of technical competence include communications, command and control, battle management, information processing, surveillance sensors, intelligence data collection and handling, solid state sciences, electromagnetics, and propagation, and electronic, maintainability, and compatibility.

END

12-86

DTIC